AFWL-TR-
68-134

HIGH ENERGY NEUTRON CROSS SECTION VALIDATION AND NEUTRON FLUX SPECTRUM USING THE HENRE SOURCE

Raymond C. Barrall

John A. Holmes

Mae Silbergeld

Stanford University

Stanford, California

Contract AF 29(601)-6780

TECHNICAL REPORT NO. AFWL-TR-68-134

March 1969

AIR FORCE WEAPONS LABORATORY

Air Force Systems Command

Kirtland Air Force Base

New Mexico

HIGH ENERGY NEUTRON CROSS SECTION VALIDATION AND NEUTRON FLUX SPECTRUM USING THE HENRE SOURCE

Raymond C. Barrall
John A. Holmes
Mae Silbergeld

Stanford University
Stanford, California
Contract AF 29(601)-6780

TECHNICAL REPORT NO. AFWL-TR-68-134

FOREWORD

This report was prepared by Stanford University, Stanford, California, under Contract AF 29(601)-6780. The research was performed under Program Elements 6.24.05.21.4 and 6.21.18.01.1, Project 1831, Task 1831 08, and was partially funded by the Army under MIPR 20-113-RE-65-3(T).

Inclusive dates of research were November 1965 to October 1968. The report was submitted 10 December 1968 by the Air Force Weapons Laboratory Project Officer, Lt Edward O. Groeber, Jr. (WLBN). Former Project Officers were Capt James K. Morrow (WLDN) and Lt Gerald P. McCarthy (WLRB).

The authors wish to express their appreciation for the encouragement and support of Dr. John DePangher, Lockheed Research Laboratory, Palo Alto, California and Dr. Donald G. Gardner, Lawrence Radiation Laboratory, Livermore, California, and to James Barrick, Gregg Carter, Vartiter Chakalian, Jerome Czech, Matthew Greer, Esther Huang, Richard Lawson, Ron Macumber, and George Seto of Stanford University for invaluable assistance in the measurements and calculations. Finally, thanks are due Fred Haywood and the HENRE Crew for operation of the HENCR accelerator, to R. Cederlund and crew at the ICT accelerator for assisting with the irradiations, and to Rex Booth for the proton recoil telescope measurements.

This technical report has been reviewed and is approved.

Edward O. Groeber, Jr.
EDWARD O. GROEBER, JR.
Lt, USAF
Project Officer

JAMES E. DIECKHONER
Capt, USAF
Chief, Bionuclear Branch

Milford D. Harris, Jr.
MILFORD D. HARRIS, JR.
Lt Col, USAF VC
Chief, Biophysics Division

ABSTRACT

(Distribution Limitation Statement No. 1)

Neutron cross sections reported by various investigators often differ far in excess of the estimates of error reported. The high neutron emission of the High Energy Neutron Reaction Experiment (HENRE) source, 10^{13} n/sec, afforded an opportunity to compare measured values of many disintegration rates in a single experiment thus eliminating some of the uncertainty necessarily associated with such measurements when based on varying standards and normalizations. From these measurements, the 14.6 MeV neutron cross sections of 24 reactions are derived. The neutron spectrum near ground level at 37 feet slant range from the HENRE source was measured by using foil data and the SAND II code. Additional measurements at the Insulated Core Transformer (ICT) accelerator at the Lawrence Radiation Laboratory, Livermore, served to confirm the HENRE results.

This page intentionally left blank.

CONTENTS

ILLUSTRATIONS

TABLES

This page intentionally left blank.

SECTION I

INTRODUCTION

The accuracy of measurements of neutron flux and spectra by foil techniques is intimately related to the accuracy of disintegration rate measurements and neutron cross sections. As numerous radioactive standards are available, disintegration rate measurements with an absolute accuracy of several percent are attainable. However, the status of neutron cross section accuracy does not permit such general confidence. One notes numerous instances in which the lack of agreement between cross sections reported by various investigators far exceeds the limits of error reported. The high neutron emission, 10^{13} n/sec of the High Energy Neutron Reaction Experiment (HENRE) source afforded an opportunity to compare measured values of many disintegration rates in a single experiment thus eliminating some of the uncertainty necessarily associated with such measurements when based on varying standards and normalizations. The high neutron emission made it possible to place foils on a rotating disc one meter from the target with a neutron flux density which varies by no more than ± 2 percent over the area of the foils. As the foils were rotating on the same radius, each foil was at the same angle during the irradiation. As a result, a consistent set of cross section data is obtained which is of considerable assistance in evaluating cross section data available in the literature. Table 1 lists the foil materials irradiated, and photon (or particle) analyzed. From these measurements, the 14.6 MeV neutron cross sections of 24 reactions are derived.

TABLE I

FOILS IRRADIATED AND REACTIONS STUDIED

Foil Material	Reaction Studied	Photon Energy Analyzed (MeV)	Photons per Disintegration
NaF	$Na^{23}(n,\gamma)Na^{24}$	1.37.	1.00
	$Na^{23}(n,2n)Na^{22}$	0.511	1.797
	$F^{19}(n,2n)F^{18}$	.511	1.94
Mg	$Mg^{24}(n,p)Na^{24}$	1.37	1.00
Al	$Al^{27}(n,\alpha)Na^{24}$	1.37	1.00
S	$S^{32}(n,p)P^{32}$	β	--
	$S^{34}(n,\alpha)Si^{31}$	β	--
NH_4Cl	$Cl^{35}(n,\alpha)P^{32}$	β	--
Mn	$Mn^{55}(n,\gamma)Mn^{56}$	0.845	0.99
	$Mn^{55}(n,2n)Mn^{54}$	0.835	1.00
Fe	$Fe^{54}(n,p)Mn^{54}$	0.835	1.00
	$Fe^{56}(n,p)Mn^{56}$	0.845	0.99
Co	$Co^{59}(n,2n)Co^{58}$	0.815	1.01
	$Co^{59}(n,\gamma)Co^{60}$	1.33	1.00
Ni	$Ni^{58}(n,np)+(n,d)Co^{57}$	.122	0.87
	$Ni^{58}(n,p)Co^{58}$	.810	0.99
	$Ni^{58}(n,2n)Ni^{57}$	1.37	0.86
Cu	$Cu^{63}(n,\alpha)Co^{60}$	1.17	1.00
	$Cu^{63}(n,\gamma)Cu^{64}$	0.511	0.38
	$Cu^{65}(n,2n)Cu^{64}$	0.511	0.38
Zn	$Zn^{64}(n,p)Cu^{64}$	0.511	0.38
Zr	$Zr^{90}(n,2n)Zr^{89}$	0.915	1.00
In	$In^{115}(n,n')In^{115m}$	0.335	0.50
	$In^{115}(n,2n)In^{114m}$	0.192	0.17
KI	$I^{127}(n,2n)I^{126}$	0.39	0.34
Au	$Au^{197}(n,\gamma)Au^{198}$	0.412	0.956
	$Au^{197}(n,2n)Au^{196}$	0.356	1.18

TABLE - Continued

Foil Material	Reaction Studied	Photon Energy Analyzed (MeV)	Photons per Disintegration
Th	$Th^{232}(n,f)$ Tracks	--	--
	$Th^{232}(n,f)Mo^{99}$ *		
MgTh	$Th^{232}(n,f)$ Tracks	--	--
U(93.15% U^{235})	$U^{235}(n,f)Mo^{99}$ *	--	--
U(99.8% U^{238})	U^{238} (n,f) Tracks	--	--
	U^{238} (n,f)Mo^{99} *	--	--

* The authors are indebted to R. Armani of Argonne National Laboratory for these measurements.

The neutron spectrum near ground level at 37 feet slant range from the HENRE source was measured using foil data and the SAND Code (Ref. 1 and 2).

Additional measurements at the Insulated Core Transformer (ICT) accelerator at the Lawrence Radiation Laboratory, Livermore, served to confirm the HENRE results. Table XIII lists the foils that were irradiated along with the resulting nuclear reactions studied.

The angular distribution of neutrons emitted by the HENRE source was measured by using sulfur pellets and nickel foils located on a 1-meter radius from the target. The reactions $S^{32}(n,p)P^{32}$, $Ni^{58}(n,p)Co^{58}$, and $Ni^{58}(n,2n)Ni^{57}$ were used.

HENRE Source

The HENRE source consists of a high-current deuteron beam striking a water cooled thick tritium target consisting of approximately 1000 curies of H^3 absorbed on a metal backing having a 14-inch diameter. Deuterons, 145 KeV in energy, strike the tritium and neutrons are produced by the $H^3(D,n)He^4$ reaction.

For brevity below, neutrons produced by this reaction are referred to as "D,T neutrons."

SECTION II

SPECIAL PROBLEMS ENCOUNTERED AND DESCRIPTION OF COUNTING TECHNIQUES

1. Multichannel Analyzer Calibration

A multichannel analyzer and 3 in. x 3 in. NaI(Tl) crystal was calibrated for photon energies ranging from 0.166 to 1.84 MeV, using standard point gamma ray sources from the National Bureau of Standards positioned 10 cm from the crystal.

To facilitate the analysis of the hundreds of measured photopeaks, several electronic calculator programs were written. Instead of measuring the total area under a photopeak, the peak count and two adjacent counts on either side of the peak (called P $\pm$ 2) are added together, and from this count, a base is subtracted. These figures, fed into the electronic calculator, enable one to obtain the measured disintegration rate. The base is selected by a consideration of the total spectrum obtained for each foil. Figure 1 shows a typical X-Y plot for the reaction $Al^{27}(n,\alpha)Na^{24}$. For this count, P $\pm$ 2 is given by (319.8 + 350.1 + 363.8 + 339.9 + 281.8) counts per minute, CPM, and the base selected is the integral of the exponential determined by the first minimum over the five channels on either side of the peak (80 CPM for this example).

The P $\pm$ 2 method for photopeak analysis was compared with the photopeak area method for measuring the activity of a number of different isotopes. In all cases excellent agreement was found. Additional counts were made with varying quantities of interfering isotopes. It was found that even with very large quantities of interfering isotopes the activity of the source can be measured with a high degree of accuracy. For example, Cs^{137} was counted with and without Co^{60} as an interfering isotope. With ten times more μCurie-minutes of Co^{60} than of Cs^{137}, the

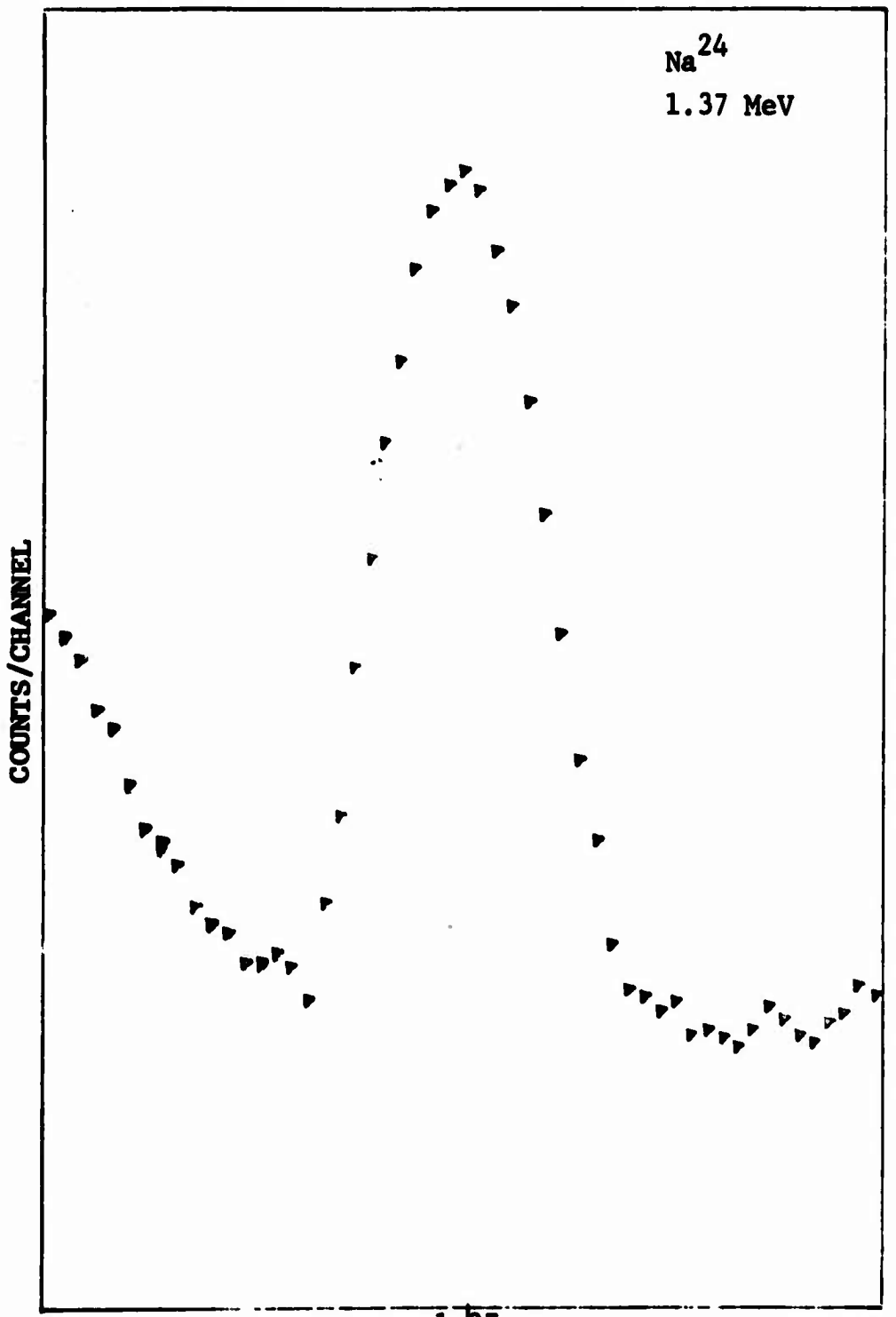

Figure 1. Typical Photopeak,
3 in. x 3 in. Foil on top of Crystal can

measured activity was only 1.29 percent lower than when Cs^{137} was counted alone. Even with forty times more μCurie-minutes of Co^{60} than of Cs^{137}, the measured activity was only 8 percent lower than when Cs^{137} was counted alone. The same data were analyzed by Dr. John DePangher at Lockheed Research Laboratory, Palo Alto, California, by using a biased Gaussian program developed by Murphy (Ref. 3) with essentially identical results.

2. Foil Size

To obtain a sufficiently large number of target atoms so that statistically significant results can be obtained, it is highly desirable to optimize the area and thickness of the foils. A standard foil size of 3 in. x 3 in. was selected because of fabrication and ease of accurate positioning for counting with the 3 in. x 3 in. NaI crystal used as the detector for pulse height analysis. Because it is desirable that both the incident neutrons and the emitted γ-rays not be attenuated appreciably, calculations were made to determine the foil thickness which would attenuate 14 MeV neutrons by 2 percent and also the foil thickness which would attenuate the γ-rays by 2 percent. Table II lists these calculated values for each foil material, along with the actual foil thickness available at the time of foil preparation.

3. Area Factor, F_A

For HENRE foils measuring 3 in. x 3 in., it was necessary to obtain an area factor, F_A, which relates a 3 in. x 3 in. source to an equivalent point source.

F_A is the quantity by which each photopeak area from a 3 in. x 3 in. foil must be divided in order to equate it to the photopeak area that would have been obtained from an equivalent point source. F_A depends on the counting distance and on the photon energy, as well as the size and shape of the foil.

TABLE II

NEUTRON AND γ-RAY FOIL ATTENUATIONS

Target Reaction	Thickness for 2%* Neutron Attenuation (in.)	Thickness for 20%** γ-Ray Attenuation (in.)	Actual Foil Thickness (in.)
Na^{23} (n,γ)Na^{24}	0.15	0.20	0.063
Na^{23} (n,2n)Na^{22}	0.15	0.064	0.063
Mg^{24} (n,p)Na^{24}	0.10	0.13	0.005
Al^{27} (nα)Na^{24}	0.080	0.083	0.016
P^{31} (n,p)Si^{31}	0.50	N.A.	0.219
S^{32} (n,p)P^{32}	0.50	N.A.	0.219
S^{34} (n,α)Si^{31}	0.50	N.A.	0.219
Cl^{35} (n,α)P^{32}	0.19	N.A.	0.156
Mn^{55} (n,γ)Mn^{56}	0.033	0.026	
Mn^{55} (n,2n)Mn^{54}	0.033	0.015	
Fe^{54} (n,p)Mn^{54}	0.035	0.014	0.020
Fe^{56} (n,p)Mn^{56}	0.035	0.023	0.020
Co^{59} (n,γ)Co^{60}	0.080	0.050	
Co^{59} (n,2n)Co^{58}	0.080	0.050	
Ni^{58} (n,p)Co^{58}	0.032	0.013	0.023
Ni^{58} (n,2n)Ni^{57}	0.032	0.017	0.023
Cu^{63} (n,γ)Cu^{64}	0.032	0.011	0.005
Cu^{65} (n,2n)Cu^{64}	0.032	0.011	0.005
Zn^{64} (n,p)Cu^{64}	0.048	0.015	0.018
Zn^{64} (n,2n)Zn^{63}	0.048	0.015	0.018

TABLE II, Cont'd

Target Reaction	Thickness for 2%* Neutron Attenuation (in.)	Thickness for 2%** γ-Ray Attenuation (in.)	Actual Foil Thickness (in.)
In^{115} (n,n')In^{115m}	0.044	0.004	0.002
I^{127} (n,2n)I^{126}	0.150	0.025	0.188
Au^{197} (n,γ)Au^{198}	0.044	0.001	0.004 and 0.000031
Th^{232} (n,f)F.P. [La^{140}]	0.048	0.015	0.001
Th^{232} (n,γ)Th^{233}	0.043	0.0015	0.001
U^{235} (n,f)F.P. [La^{140}]	0.050	0.015	
U^{238} (n,f)F.P. [La^{140}]	0.048	0.015	0.002
U^{238} (n,γ)U^{239}	0.083	0.00038	0.002

* Simple Collision Attenuation Using Total Cross Section.

**Simple Attenuation Using Total Foil as Absorber.

In order to determine F_A for a given counting distance D , each standard source was counted at the central position and at varying lateral distances, r , from the crystal center. For each standard source, photopeak areas were thus obtained at the central position and at varying lateral distances. If the foil is considered as being composed of many small regions each with an area A(r) then F_A is given by

$$F_A = \frac{\sum \frac{N(r)}{N_o} A(r)}{\sum A(r)}$$

where N(r) = photopeak area with source at a lateral distance, r , from the central axis, and N_o = photopeak area with the source at the same counting distance but on the central axis.

For a 3 in. x 3 in. foil, the summation extends from r = o to r = 2.12 in. (the corner positions). Thus one obtains

$$F_A = \frac{\sum_{r=o}^{r=2.12} \frac{N(r)}{N_o} A(r)}{9 \text{ in}^2}$$

By numerical integration, F_A was measured for each standard source at a counting distance of 10 cm and with the source on top of the crystal can.

By using each standard source, numerical integration was performed and F_A thus measured as a function of photon energy. Measurements were made for counting distance of 10 cm from the crystal and on top of the crystal can.

4. Distance Factor, F_D

To obtain sufficiently large count rates, it was necessary to count some of the foils on the top of the crystal can. This introduced the complication of coincidence effects

for many isotopes. For each isotope it became necessary to obtain a distance factor F_D, in order to relate the photopeak area from the top of the crystal can, to that which would have been obtained if the foil had been counted at 10 cm.

An additional correction was needed to account for the foil thickness. When the foil was placed 10 cm from the crystal, the actual counting distance ranged from 10 cm to 10 + t cm where t = foil thickness. Similarly, when the foil was placed on top of the crystal can (actually 0.318 cm from the crystal face) the actual counting distance ranged from 0.318 to 0.318 + t cm. To correct for foil thickness, it is necessary to know how the efficiency of the crystal varies with counting distance. Heath (Ref. 4) has plotted a series of curves showing total absolute efficiency for a 3 in. x 3 in. NaI(Tl) crystal as a function of γ-ray energy for selected counting distances. The distance factor with foil at 10 cm is given by

$$F_D = \frac{\text{Efficiency at } (10 + t/2)\,\text{cm}}{\text{Efficiency at 10 cm}}$$

With the foil on top of the crystal can the distance factor is given by

$$F_D = \frac{A_T \text{ Efficiency at } (0.318 + t/2)\,\text{cm}}{A_{10} \text{ Efficiency at } 0.318 \text{ cm}}$$

where A_T = photopeak area from a point source on top of the crystal can, and A_{10} = photopeak area from the same source at 10 cm.

For each foil, the measured photopeak area must be divided by F_D in order to obtain the equivalent photopeak area that would have been obtained at 10 cm.

5. Attenuation Factor, F_a

A further correction factor, F_a accounts for attenuation of photons within the material of the foil itself. The amount of attenuation is determined by the energy of the emitted photon and by the foil thickness. The measured photopeak area for each

foil must be multiplied by F_a in order to obtain the photopeak area that would have been measured had there been no attenuation. As the corrections are small it is sufficiently accurate to use F_a calculated for each foil from the relation:

$$F_a = 1 + 0.02 \left(\frac{\text{Foil Thickness}}{\text{Thickness for 2\% } \gamma\text{-ray attenuation}}\right)$$

Table II lists the thickness for each foil reaction that attenuates the emitted γ-rays by 2 percent.

6. Coincidence Factor, F_c

For those isotopes having coincidence losses caused by a secondary photon, the measured photopeak area was divided by a coincidence factor, F_c, which was calculated from the relation:

$$F_c = 1 - (G\, \varepsilon_t\, e^{-\mu x})$$

where G = number of secondary photons per disintegration
ε_t = absolute total efficiency of the crystal for the secondary photon
$e^{-\mu x}$ = transmission of the crystal canning material for the secondary photon energy.

7. Fission Track Measurements

Foils of U^{238}, U^{235}, Th^{232}, and MgTh alloy were sandwiched between thin (approximately 1/64 in.) Lexan plastic and placed in the field of irradiation at each HENRE run. After irradiation, the Lexan sheets were etched in a 6 N solution of KOH at 150°F for 15 minutes, then rinsed in distilled water and blotted dry with lens tissue. Each Lexan sheet was then viewed through a microscope and the fission tracks counted. The number of tracks/cm^2 was thus obtained. The value of 1.17×10^{-5} tracks/n-barn for foils of infinite thickness reported by Pretre, Tochilin, and Goldstein (Ref. 5) was used in order to determine a cross section value for the fission foils.

TABLE III

Irradiation Times, HENRE
Run No. 17, 11/11/66.

Spark Number	Time Off PST	Length of Run (sec.)	Down Time (sec.)	Beam Current (ma)	Avg. ct/sec-ma w/ dead time correction	Continuous Total cts.
1	12:16 - 07	63	28	---	---	---
2	12:17 - 04	30	20	---	---	---
3	12:22 - 10	285	35	---	92.8	6,254,952
4	12:23 - 20	35	79	300	98.3	7,217,600
5	12:28 - 17	218	32	300	122.5	14,580,000
6	12:29 - 21	33	30	300	95.7	15,466,000
7	12:33 - 36	225	72	320	110.1	22,777,000
8	12:42 - 45	477	68	340	102.4	38,107,000
9	12:57 - 03	791	167	350	80.6	59,000,000
10	13:00 - 00	10	22	---	---	---
11	13:02 - 30	128	41	350	63.2	61,687,000
12	13:05 - 00	109	150	350	59.8	63,856,000
13	13:08 - 16	46	29	350	61.3	64,793,000
14	13:09 - 00	15	24	---	---	65,024,000
15	13:11 - 14	109	47	350	59.3	67,175,000
16	13:15 - 15	194	358	---	59.3	71,004,000
17	13:23 - 54	162	23	350	53.4	73,900,000
18	13:25 - 42	85	43	350	48.7	75,290,000
19	13:26 - 57	32	82	---	---	75,643,000
20	13:33 - 06	287	32	350	50.9	80,543,000
21	13:36 - 04	146	47	350	47.1	82,854,000
22	13:37 - 43	52	40	350	---	83,604,000
23	13:42 - 54	271	57	350	45.3	87,739,000

TABLE III, Cont'd

Spark Number	Time Off PST	Length of Run (sec.)	Down Time (sec.)	Beam Current (ma)	Avg. ct/sec-ma w/ dead time correction	Continuous Total cts.
24	13:55 - 46	715	62	335	42.0	97,449,000
25	13:57 - 49	61	71	350	35.8	98,191,000
26	14:01 - 27	147	67	345	36.8	99,998,000
27	14:02 - 49	15	58	---	---	100,126,000
28	14:04 - 01	10	72	---	---	100,228,000
29	14:06 - 00	47	121	250	---	100,416,000
30	14:12 - 42	281	2008	330	34.4	103,519,000
Shut down after spark off to clean corona dome and column.						
31	14:35 - 45	35	41	---	---	103,792,000
32	14:39 - 54	208	53	erratic	---	104,943,000
33	14:41 - 47	60	39	---	---	105,509,000
34	14:43 - 41	75	30	---	---	106,073,000
35	14:46 - 36	145	32	300	30.8	107,382,000
36	14:51 - 58	290	35	310	30.4	110,055,000
37	15:00 - 52	499	88	310	33.3	115,078,000
38	15:21 - 25	1145	48	310	40.6	129,045,000
39	15:53 - 12	1859	205	310	43.9	153,520,000
40	15:58 - 15	98	67	310	44.5	154,827,000
41	16:00 - 55	93	31	310	42.7	156,018,000
42	16:02 - 46	80	66	310	41.5	157,015,000
43	16:37 - 26	2016	63	300	43.6	182,516,000
44	17:00 - 34	1325	60	300	41.6	198,537,000
45	17:14 - 01	747	---	250	37.8	205,422,000

SECTION III

NEUTRON EMISSION OF HENRE TARGET AS A FUNCTION OF TIME

1. Run No. 17, 11/11/66

Table III gives the data obtained from the fission counter located above the HENRE accelerator and used to provide normalization of neutron emission during and between accelerator runs at varying times. The design of the accelerator is such that the accelerator is shut down frequently by sparking. During Run No. 17, 45 increments of irradiation occurred. The neutron emission as a function of time is not constant because of a number of factors:

a. The approximately 1,000 curie tritium targets lose tritium because of burn up in the intense deuteron beam of the accelerator.

b. Localized heating of the target may contribute to tritium loss.

c. Impurity molecules may be accelerated and deposited on the tritium target, thus attenuating the deuteron beam. Because the energy of the deuteron beam is close to the threshold for the D,T reaction, attenuation or energy loss may result in a deuteron energy too low to initiate the D,T reaction.

d. Some deuterium builds up on the target, probably increasing with time, which then leads to neutron emission from the D,D, reaction.

To relate the activity of neutron-induced reactions and their products having varying half-lives to the neutron emission, it is necessary to calculate and sum 45 increments of build up, $(1 - e^{-\lambda t})$, and decay $(e^{-\lambda t}2)$. A convenience

adopted was to define a correction factor, CF, which when multiplied by the disintegration rate measured transforms all the data to that which would have been obtained by an irradiation at constant flux density and of duration equal to the sum of the "on times" of the time increments for a given run. Such corrected values of disintegration rates may then be used in the usual activation formulas.

$$CF = \frac{\lambda[\Sigma C(I)](1 - e^{-\lambda \Sigma T(I)})/\lambda \Sigma T(I)}{\sum C[I] \frac{\lambda(1 - e^{-T(I)})}{\lambda T(I)} e^{-(T_f - T_i)}}$$

λ is the decay constant for a particular half-life, $\log_e 2/T_{\frac{1}{2}}$.

C(I) is the accumulated count of the fission counter in an interval of time, T(I).

T(I) is the "on time" of a given time interval.

T_f is the final time, the clock time at the end of the last time interval, T(I).

T_i is the clock time at the end of a time interval, T(I).

The correction factors for Run No. 17 are tabulated in Table IV*.

2. Run No. 40, 7/10/67

Irradiation time data are tabulated for Run No. 40 in Table V. The 40 increments of irradiation were treated in the same manner as described for Run No. 17. Table VI summarizes the results for various half-lives, and Figure 2 shows these data in graphical form.

*The assistance of Dr. John DePangher in providing these calculations is gratefully acknowledged.

TABLE IV

Irradiation Time Correction Factors for HENRE Run 17

Nuclide	T 1/2 (days)	Correction Factor
Ni^{57}	1.5	1.016
P^{32}	14.2	1.0017
Mn^{54}	311.9	1.00008
In^{115m}	.1863	1.12049
Zr^{89}	3.292	1.00732
I^{127}	12.8	1.00189
Au^{198}	2.7	1.00892
Cu^{64}	.5333	1.04436
Na^{24}	.625	1.03798
Co^{60}	1913.	1.000013
Sc^{46}	84.1	1.000288
Sc^{47}	3.42	1.00705
Sc^{48}	1.84	1.013066
Co^{58}	71.3	1.000340
Co^{57}	267	1.000091
Mn^{56}	.1075	1.193752
Au^{196}	6.3	1.003834
Na^{22}	941.7	1.000026

TABLE V

Irradiation Times, HENRE

Run No. 40, 7/10/67.

Spark Number	Machine Off Clock Time	Length of Run (mins.)	Down Time (mins.)	Total cts. during run w/ dead time cor.	Continuous Total cts.
1	11:03.0	1.0	.3	47,598	47,598
2	11:04.0	.7	.3	59,720	107,318
3	11:07.0	2.6	.3	557,126	664,444
4	11:14.5	7.2	.8	2,558,809	3,223,253
5	11:20.6	4.9	.4	1,912,819	5,136,072
6	11:27.0	6.3	.5	2,437,183	7,573,255
7	11:35.3	7.9	---	2,545,040	10,118,295
8	11:53.9	5.8	.5	1,770,104	11,888,399
9	11:54.8	.4	.3	112,351	12,000,750
10	11:55.3	.2	.4	25,136	12,025,886
11	11:56.2	.6	.3	125,120	12, 151,006
12	11:58.9	2.4	.5	591,245	12,742,251
13	12:00.3	.9	.3	207,044	12,949,295
14	12:02.3	1.7	.3	256,245	13,405,540
15	12:03.7	1.2	.3	259,407	13,664,947
16	12:04.2	.2	.3	30,196	13,695,143
17	12:04.8	.3	1.3	35,178	13,730,321
18	12:06.2	.1	.3	11,053	13,741,374
19	12:06.8	.3	.3	52,393	13,793,767
20	12:08.6	1.5	.2	342,353	14,136,120
21	12:09.6	.7	.4	167,723	14,303,843
22	12:12.6	2.7	.3	605,834	14,909,677
23	12:13.2	.3	.3	55,440	14,965,117

TABLE V, Cont'd

Spark Number	Machine Off Clock Time	Length of Run (mins.)	Down Time (mins.)	Total cts. during run w/ dead time cor.	Continuous Total cts.
24	12:16.5	3.1	.4	664,108	15,629,225
25	12:17.2	.3	.3	37,199	15,666,424
26	12:23.9	6.4	---	1,382,827	17,049,251
27	12:34.8	1.7	.3	278,970	17,328,221
28	12:35.7	.6	.3	85,525	17,413,746
29	12:36.3	.2	.2	27,159	17,440,905
30	12:36.5	.2	.3	15,049	17,455,954
31	12:37.5	.7	.2	96,574	17,552,528
32	12:37.9	.1	.4	12,063	17,564,591
33	12:39.1	.8	.3	11,671	17,676,262
34	12:40.6	1.3	.3	233,808	17,910,070
35	12:41.6	.6	---	107,833	18,017,903
36	12:49.6	.6	.3	95,656	18,113,559
37	12:50.1	.2	.2	28,171	18,141,730
38	12:50.6	.2	.3	40,350	18,182,080
39	12:52.1	1.3	.4	224,670	18,406,750
40	12:53.7	1.2	---	217,698	18,824,448

TABLE VI

Irradiation Time Correction Factors for HENRE

Run 40

Nuclide	T 1/2 (days)	Correction Factor
Ni^{57}	1.5	1.01108
P^{32}	14.2	1.00117
Mn^{54}	311.9	1.00005
In^{115m}	.1863	1.09116
Zr^{89}	3.292	1.00504
I^{127}	12.8	1.00130
Au^{198}	2.7	1.00615
Au^{196}	6.3	1.00263
Cu^{64}	.5333	1.03135
Na^{24}	.625	1.02671
Na^{22}	941.7	1.00002
Co^{60}	1913.	1.00001
Sc^{46}	84.1	1.00020
Sc^{47}	3.42	1.00485
Sc^{48}	1.84	1.00903
Co^{58}	71.3	1.00023
Co^{57}	267	1.00006
Mn^{56}	.1075	1.160583

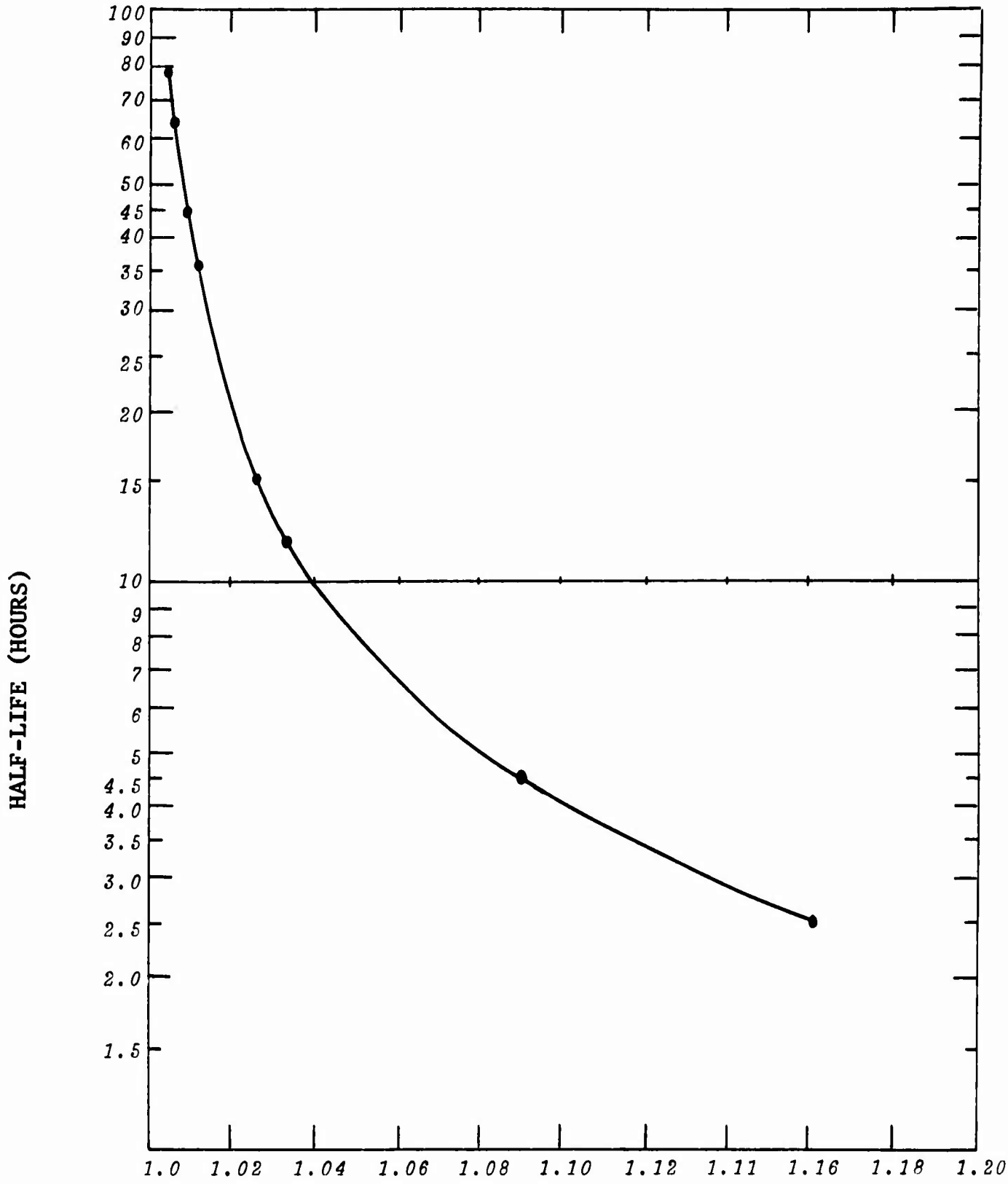

Figure 2. Irradiation Time Correction Factors for HENRE, Run No. 40.

SECTION IV

HENRE RUN NO. 17, 11/11/66

1. General Description

This was a 3.64-hr irradiation during which foils were irradiated at two different distances from the neutron source, viz. at 1-meter and at 37 feet.

At 1- meter from the target, there was a copper tube arc on which were placed 95 sulfur pellets and 3 nickel foils, as shown in Figure 3.

At 37 feet from the target were placed all the foils listed in Table I. These foils were 11 inches above the ground and at a horizontal distance of 27 feet from the center of the target. The neutron source was 27 feet above the ground.

2. Angular Distribution of Source Neutrons, Measured at 1 Meter

In order to measure neutron emission from the HENRE source as a function of angle, sulfur pellets and nickel foils were irradiated. Ninety-five sulfur pellets were placed on a 1-meter arc around the target source as shown in Figure 3. All pellets were at a distance of 1 meter from the neutron source, but at angles ranging from 0° to 100°. Three nickel foils were placed at angles of 0°, 45°, and 90°, respectively, from the target source. The position of these nickel foils corresponded to sulfur pellets numbered 48-49, 28-29, and 3-4-5. After irradiation, all pellets were sublimed and the activities of Si^{31} and of P^{32} measured in an automatic beta scintillation counter. Activities of Co^{58} and of Ni^{57} were measured in a multichannel analyzer. Table VII lists the average activities, decay-corrected to time at end of irradiation. The activity in those foils at 0° and at 45° was approximately the same for each reaction. At 90°, the activity was much less. Note that at all angles, the activity measured by the reaction $Ni^{58}(n,2n)Ni^{57}$ correspond to a much lower

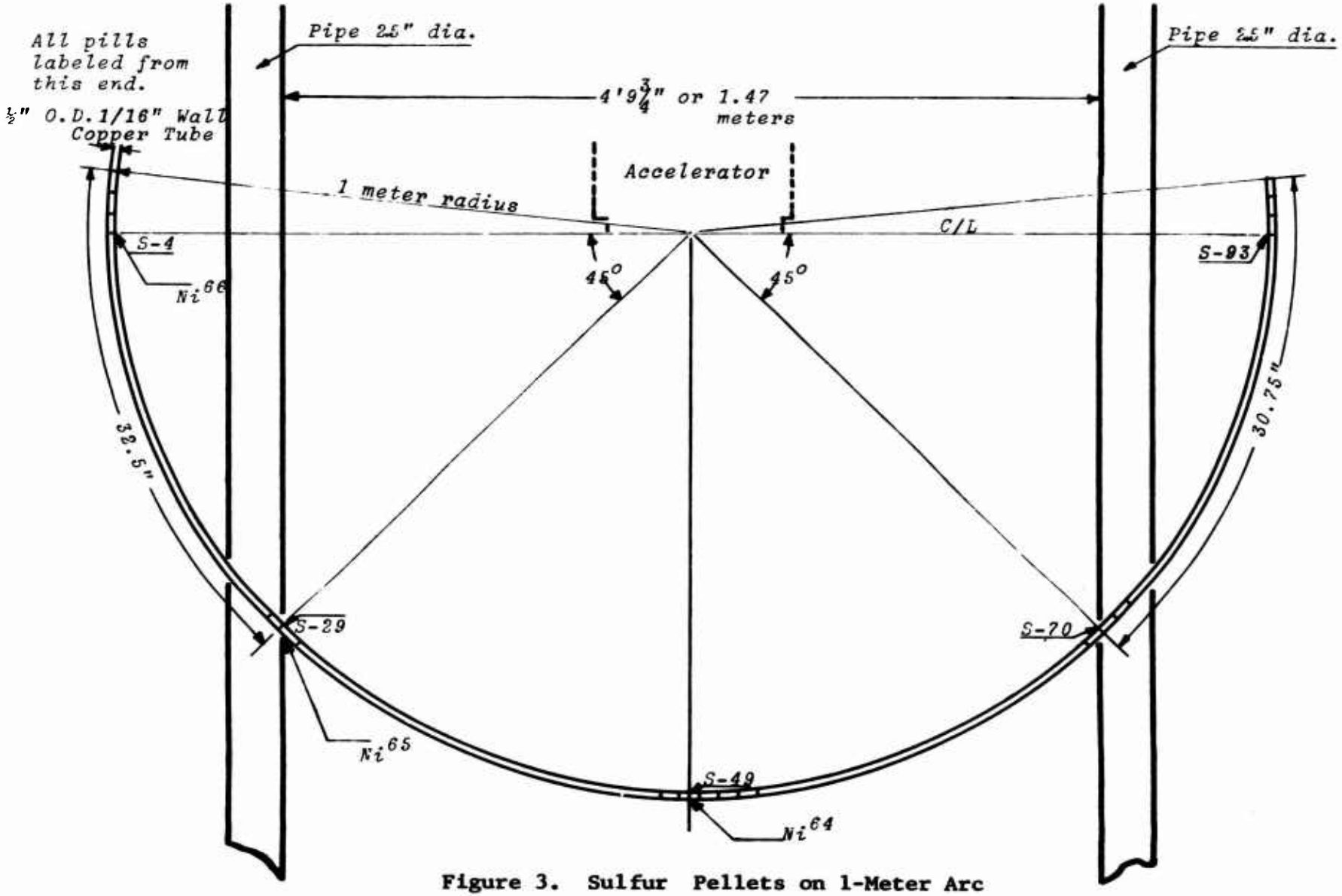

Figure 3. Sulfur Pellets on 1-Meter Arc
Run No. 17, 11/11/66, HENRE Test Site

TABLE VII

ACTIVITIES IN SAMPLES IRRADIATED AT 1 METER

HENRE RUN NO. 17, 11/11/66.

Angle	Reaction	Decay Corrected Activity (DPM/gram)	Activity at Saturation (DPS/nucleus$\times 10^{18}$)	Flux Density* (n/cm^2-sec$\times 10^{-6}$)
0	$Ni^{58}(n,p)Co^{58}$	16858	27.4	77.8
	$Ni^{58}(n,2n)Ni^{57}$	48.3	1.79	55.4
	$S^{32}(n,p)P^{32}$	136300	17.3	75.4
	$S^{32}(n,\alpha)Si^{31}$	278500	9.48	68.3
45°	$Ni^{58}(n,p)Co^{58}$	17302	27.9	79.1
	$Ni^{58}(n,2n)Ni^{57}$	48645	1.81	55.9
	$S^{32}(n,p)P^{32}$	139500	17.7	77.2
90°	$Ni^{58}(n,p)Co^{58}$	6710	10.90	31.0
	$Ni^{58}(n,2n)Ni^{57}$	9496	0.353	10.9
	$S^{32}(n,p)P^{32}$	51200	6.49	28.3

* Calculated by assuming all activity caused by 14.5 neutrons, and by using the following values for cross section:

$Ni^{58}(n,p)Co^{58}$ ----- .352 Barns
$Ni^{58}(n,2n)Ni^{57}$ ----- .0308 "
$S^{32}(n,p)P^{32}$ ----- .2292 "
$S^{32}(n,\alpha)Si^{31}$ ----- .1346 "

flux density than for the other reactions. This might be an indication of the presence of low-energy neutrons, which could not initiate the reaction $Ni^{58}(n,2n)Ni^{57}$, because the threshold of energy for this reaction is approximately 13 MeV. All the other reactions, however, are responsive to low-energy neutrons (1 to 3 MeV).

Figure 4 shows decay-corrected activity in the sulfur pellets measured as a function of angle. Each point plotted on the graph is the average of three separate determinations based on counting sublimed P^{32} samples at three considerably different times. The data show some relatively minor variations and few rather marked variations. The suggestion of symmetry is apparent from the graph. The low activities at approximately $\pm 52°$ are thought to be the result of the method of insulating the arc from the supporting pipes, which probably resulted in appreciable shielding of the sulfur pellets. Note that in the geometry employed, the total cross section tends to act as a removal cross section, because any scattering event results in a change in direction of the neutron. The neutron travels a large distance in air before experiencing another encounter and another change in direction. Thus there is an extremely low probability of the neutron returning to the sample. There is no apparent explanation for the marked decrease in activity noted at $\pm 20°$. A study of the drawings of the target did not lead to any reasonable explanation (e.g., attenuation in the target). While not understood, these apparent dips at $\pm 20°$ are thought to be spurious.

3. Neutron Spectrum with Ground Scatter, Measured at 37 ft.

Foils were positioned 11 inches above ground to provide an irradiation in which considerable ground scatter influences the neutron spectrum. The foils 37 ft from the neutron source, were to receive only about 1 percent of the neutron flux to be received by similar foils to be irradiated at 1 meter (Run No. 40).

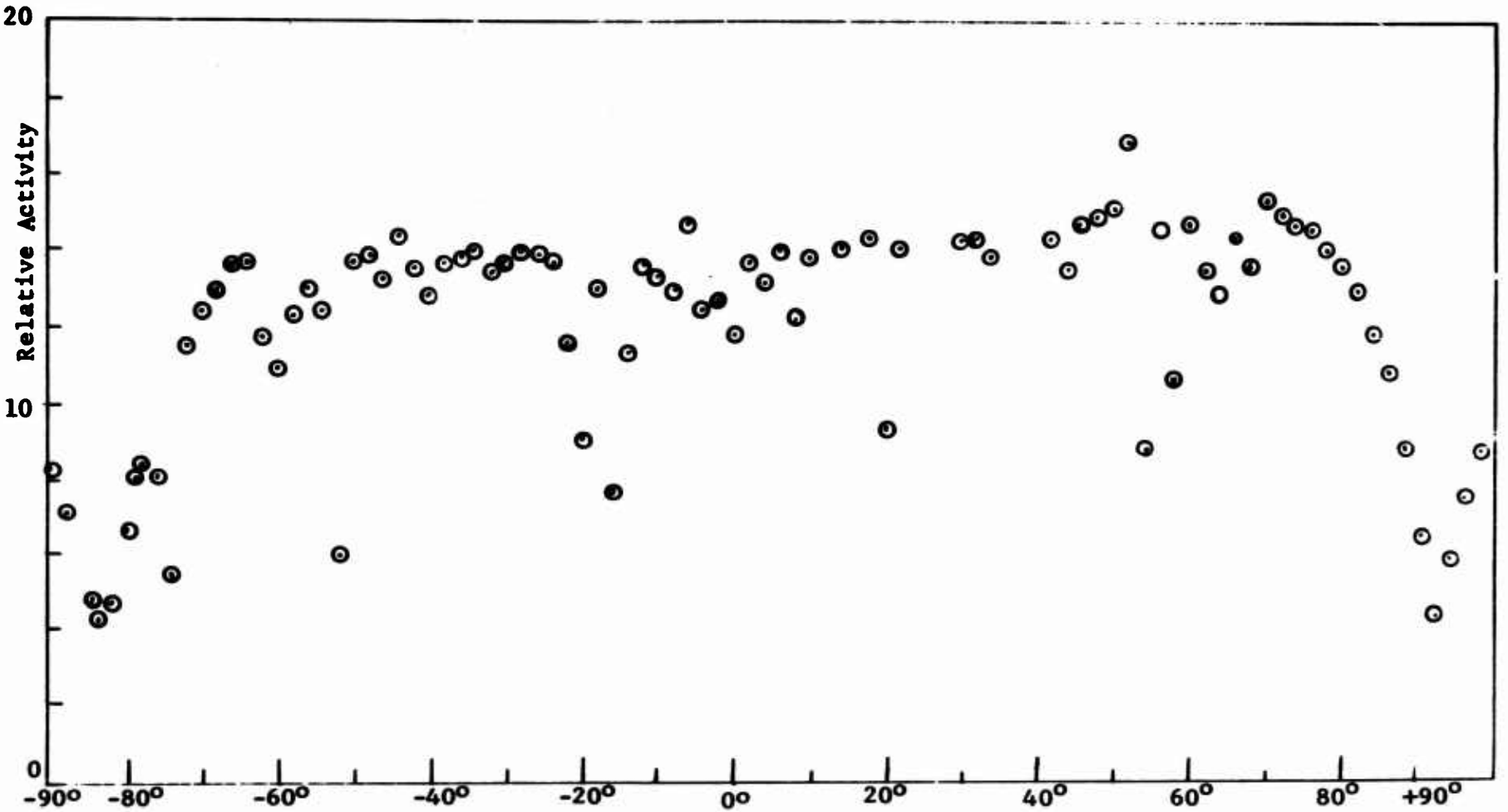

Figure 4. $S^{32}(n,p)P^{32}$ on 1-Meter Arc.
Run No. 17, 11/11/66, HENRE Test Site.

After irradiation, activities of the foils were measured. Table VIII lists the activities, decay corrected to time at end of irradiation, and the corresponding activity at saturation for each reaction. These data were used as input to the SAND II Code. Eight different spectra were used as input to the SAND II Code and iteration performed. A persistent result from each test spectrum was the unexpectedly high total number of neutrons having energies greater than Cd cutoff. A typical result was one in which the number of neutrons was of the order of 6×10^6 n/cm^2-sec. These low-energy results may have been influenced by the fact that the cross sections for most of the (n,γ) reactions are poorly known in the 14 MeV region. Most of the high-energy reactions gave a rather consistent result of approximately 0.6×10^6 neutrons/cm-sec at the 37-ft slant range. Figure 5 shows a typical result of differential flux vs energy as obtained from the SAND II Code.

TABLE VIII

ACTIVITIES IN FOILS IRRADIATED AT 37 FT
HENRE TEST SITE, RUN NO. 17, 11/11/66.

Reaction	Decay Corrected Activity (DPM/μgram)	Saturation Activity (DPS/nucleus x 10^{19})
$Na^{23}(n,2n)Na^{22}$	.00000819	.466
$Na^{23}(n,\gamma)Na^{24}$	.00110	.0450
$Mg^{24}(n,p)Na^{24}$	.0221	1.227
$Al^{27}(n,\alpha)Na^{24}$	.0168	.809
$S^{32}(n,p)P^{32}$	.001244	1.571
$Cl^{35}(n,\alpha)P^{32}$	.3513	---
$Mn^{55}(n,\gamma)Mn^{56}$	.0672	1.63
$Mn^{55}(n,2n)Mn^{54}$	.0000967	4.39
$Fe^{54}(n,p)Mn^{54}$	.00000338	2.67
$Fe^{56}(n,p)Mn^{56}$	.0340	.918
$Zn^{64}(n,p)Cu^{64}$	.006356	1.31
$Zr^{90}(n,2n)Zr^{89}$	.00242	3.83
$In^{115}(n,n')In^{115m}$	.0238	1.84
$I^{127}(n,2n)I^{126}$	.00186	8.28
$Au^{197}(n,\gamma)Au^{198}$	.136	195.
$Au^{197}(n,\gamma)Au^{198}$-$B^{10}$	.0092	13.3
$Cu^{63}(n,\gamma)Cu^{64}$-Cd	.02120	2.92
$Cu^{63}(n,\gamma)Cu^{64}$-B^{10}	.02683	3.69
$Ni^{58}(n,2n)Ni^{57}$	.000558	.197
$Ni^{58}(n,p)Co^{58}$	.000202	3.29
$Co^{59}(n,2n)Co^{58}$	.000412	3.29
$Co^{59}(n,\gamma)Co^{60}$	.00000625	1.86
$Th^{232}(n,f)$Tracks	4.430×10^{4}*	

*Tracks/cm^2

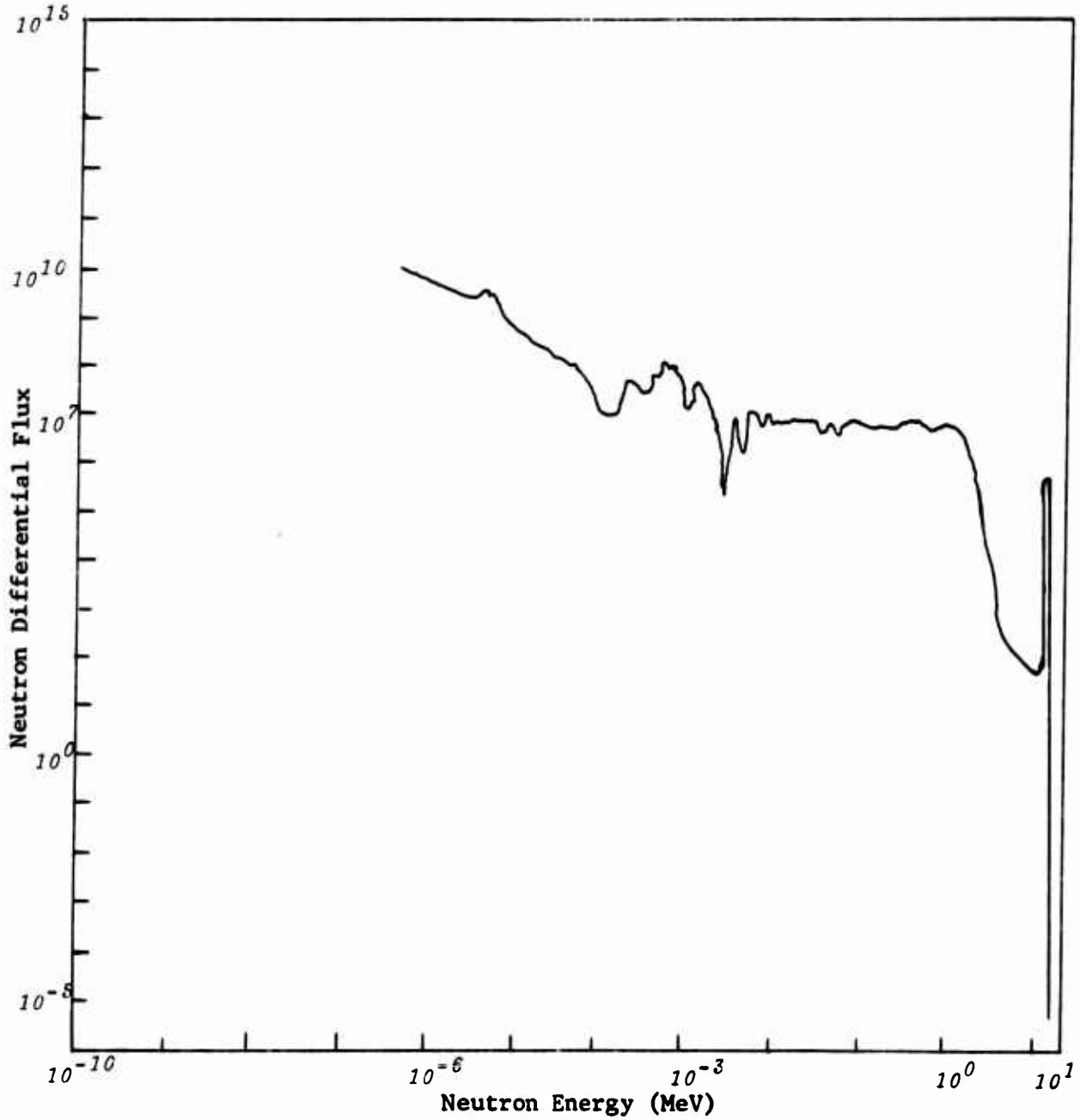

Figure 5. HENRE Neutron Spectrum at 37 ft Slant Range.
Run No. 17, 11/11/67.

SECTION V

RUN NUMBER 40, HENRE TEST SITE, 7/10/67

1. General Description

Figure 6 shows the experimental arrangement for this 1.1567-hour irradiation. Note that all irradiations were performed at a height of more than 20 ft above the ground, thus minimizing ground scatter. In order to measure the neutron cross section for those nuclear reactions listed in Table I, 3 in. x 3 in. foils were fastened to a large rotating disc placed one meter from the target. The disc consisted of a 1/8 in. aluminum plate covered with 0.030 inches of cadmium. During irradiation the disc was rotated at 5 revolutions per minute, thereby assuring that all foils received the same neutron flux.

In addition to the irradiations just described, the following foils were irradiated:

a. Nickel foils and sulfur pellets were placed along the radius of the large rotating disc.

b. A nickel strip was placed in contact with the center of the target.

c. Gold foils were placed within varying amounts of polyethylene moderator (8 ft 2 in. from target center).

d. Foils of copper, gold, nickel, and sulfur were placed inside boron balls on a small rotating disc at a distance of 1.24 meters from the target source.

2. Relative Neutron Energy Distribution Across the Radius of the Large Disc.

In order to measure the neutron energy distribution, 20 nickel foils and 15 sulfur pellets were wrapped in aluminum foil and placed in a straight line along the radius of the large

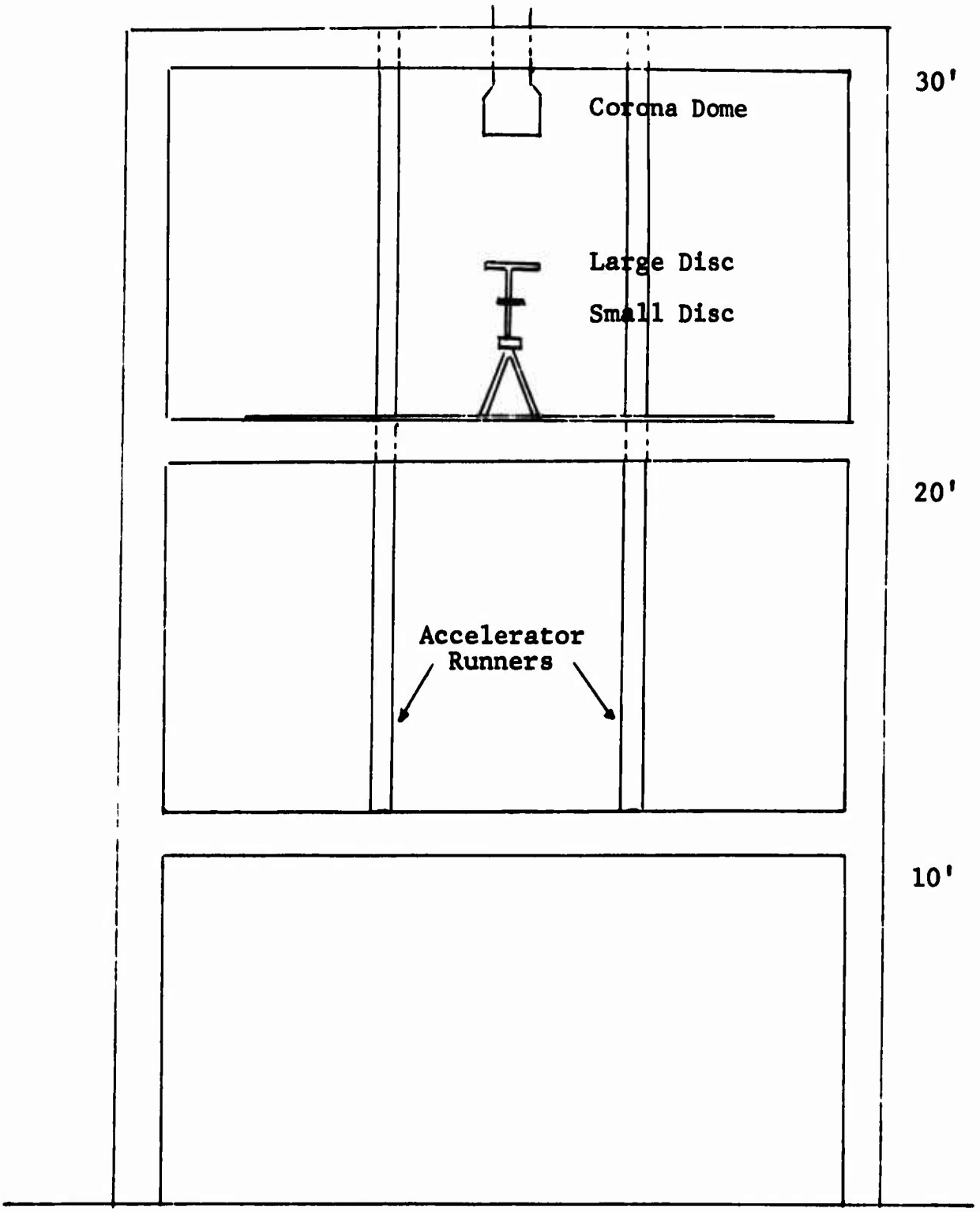

Figure 6. Experimental Setup for Run No. 40, HENRE, 7/10/67.

rotating disc. The nickel foils weighed between 0.9145 and 0.935 grams and measured 0.4443 ± 0.0005 inches in diameter. The sulfur pellets weighed between 0.2661 and 0.3351 grams and were approximately 0.25 inches in diameter. The reactions $S^{32}(n,p)P^{32}$, $Ni^{58}(n,p)Co^{58}$, and $Ni^{58}(n,2n)Ni^{57}$ were studied across the radius of the disc. Figure 7 lists the relative intensity product activity of each of these three nuclear reactions across the radius of the disc.

Because this ratio is strongly dependent on neutron energy, the constant ratio of activity of Ni^{57} relative to Co^{58} indicates that there was no neutron energy gradient over the foil positions. Thus it may be inferred that

a. The 3 in. x 3 in. foils were in a neutron flux that was uniform to within ±2 percent.

b. All portions of any 3 in. x 3 in. foil were exposed to neutrons having the same energy.

3. Emitted Neutron Energy Distribution

To refine previous calculations of the emitted energy distribution, a strip of nickel was irradiated while lying directly in contact with the target and on the diameter. The nickel strip was 11-15/16 inches long, 0.13 inches wide, and 0.13 inches thick.

Following irradiation, the large nickel strip was subdivided into twelve approximately 1 in. strips. The activity resulting from the reactions $Ni^{58}(n,p)Co^{58}$ and $Ni^{58}(n,2n)Ni^{57}$ was then measured in each strip. Table IX lists the activities of Co^{58} and Ni^{57}, decay-corrected to time at end of irradiation, as well as the corresponding saturation activities and ratios of saturated activities. Figures 8 and 9 show the activites of Co^{58} and Ni^{57} as a function of distance from the center of the target. One notes that the activities of both Ni^{57} and Co^{58} increase toward the center of the strip. This

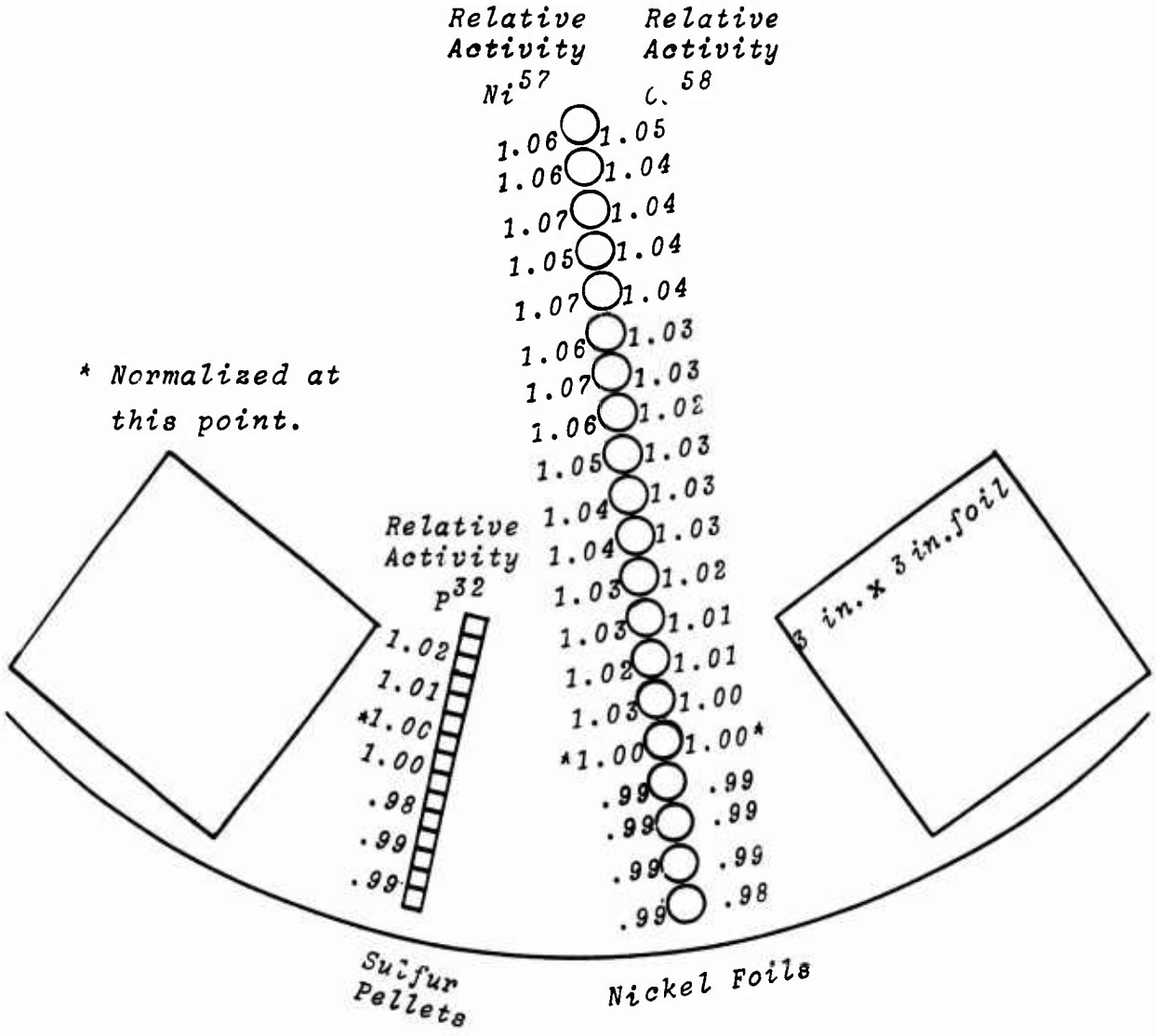

Figure 7. Neutron Distribution Across 3 in. x 3 in. Foils on Rotating Disc, HENRE Run No. 40, 7/10/67.

TABLE IX

DECAY-CORRECTED ACTIVITIES IN NICKEL STRIP NEXT TO TARGET,
RUN NO. 40, 7/10/67.

Strip No.	Ni^{57} Activity (DPM/gram) x 10^{-5}	Co^{58} Activity (DPM/gram) x 10^{-5}	Co^{58} Sat. Activity (DPS/nucleus x 10^{16})	Ni^{57} Sat. Activity (DPS/nucleus x 10^{17})	$\frac{\text{Sat. Activity } Co^{58}}{\text{Sat. Activity } Ni^{57}}$
1	4.51	1.41	7.19	4.90	14.7
2	5.69	1.78	9.09	6.18	14.7
3	8.92	2.69	13.8	9.69	14.2
4	15.4	4.30	21.9	16.7	13.1
5	20.6	5.73	29.2	22.4	13.0
6	18.5	5.46	27.9	20.0	13.9
7	16.1	4.79	24.4	17.5	14.0
8	13.2	3.99	20.4	14.3	14.2
9	9.78	2.88	14.7	10.6	13.8
10	6.75	2.12	10.8	7.34	14.8
11	4.31	1.47	7.51	4.68	16.0
12	5.04	1.62	8.27	5.47	15.1

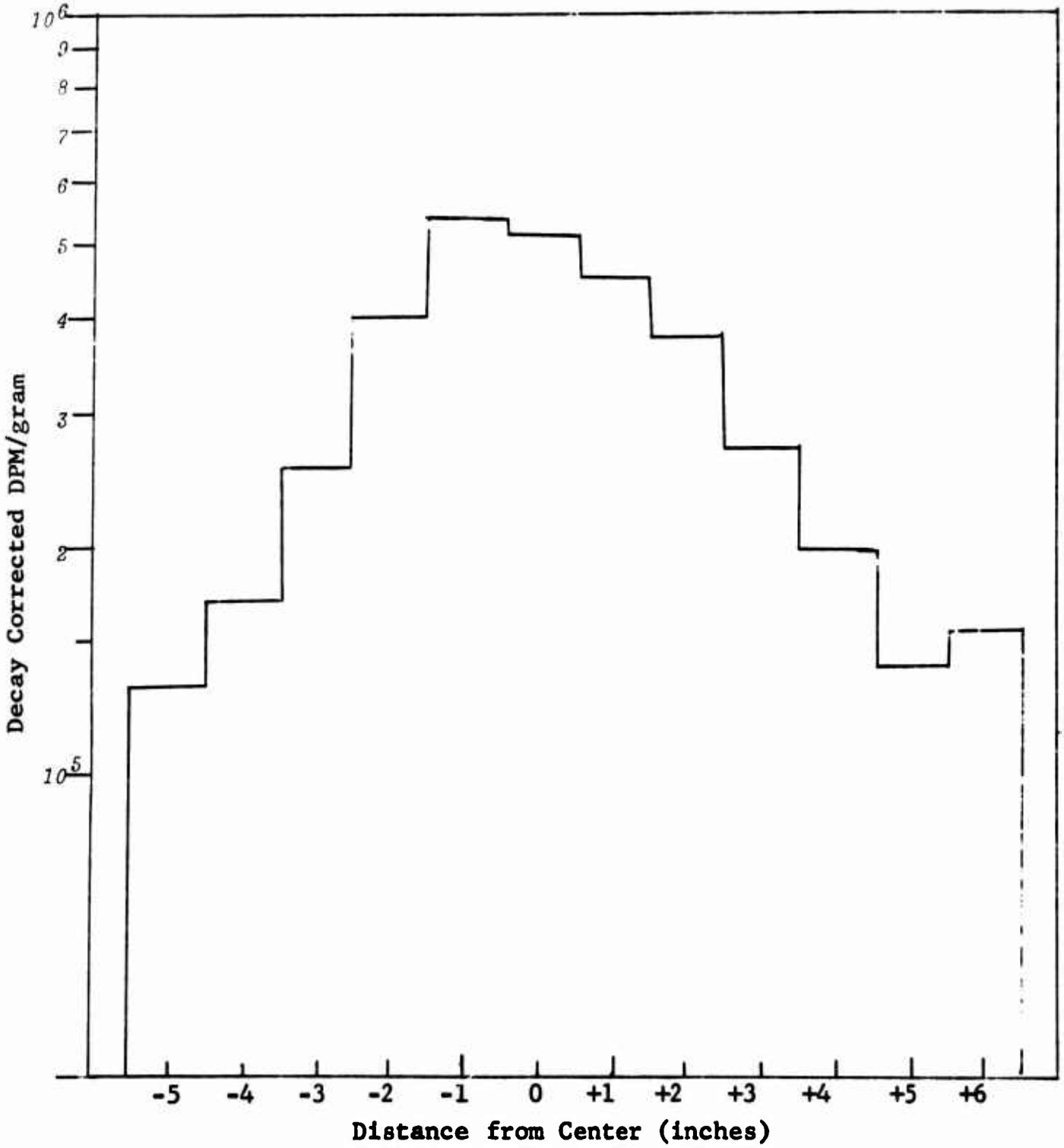

Figure 8. Co^{58} Activity from $Ni^{58}(n,p)Co^{58}$ Across Radius of Target, 7/10/67

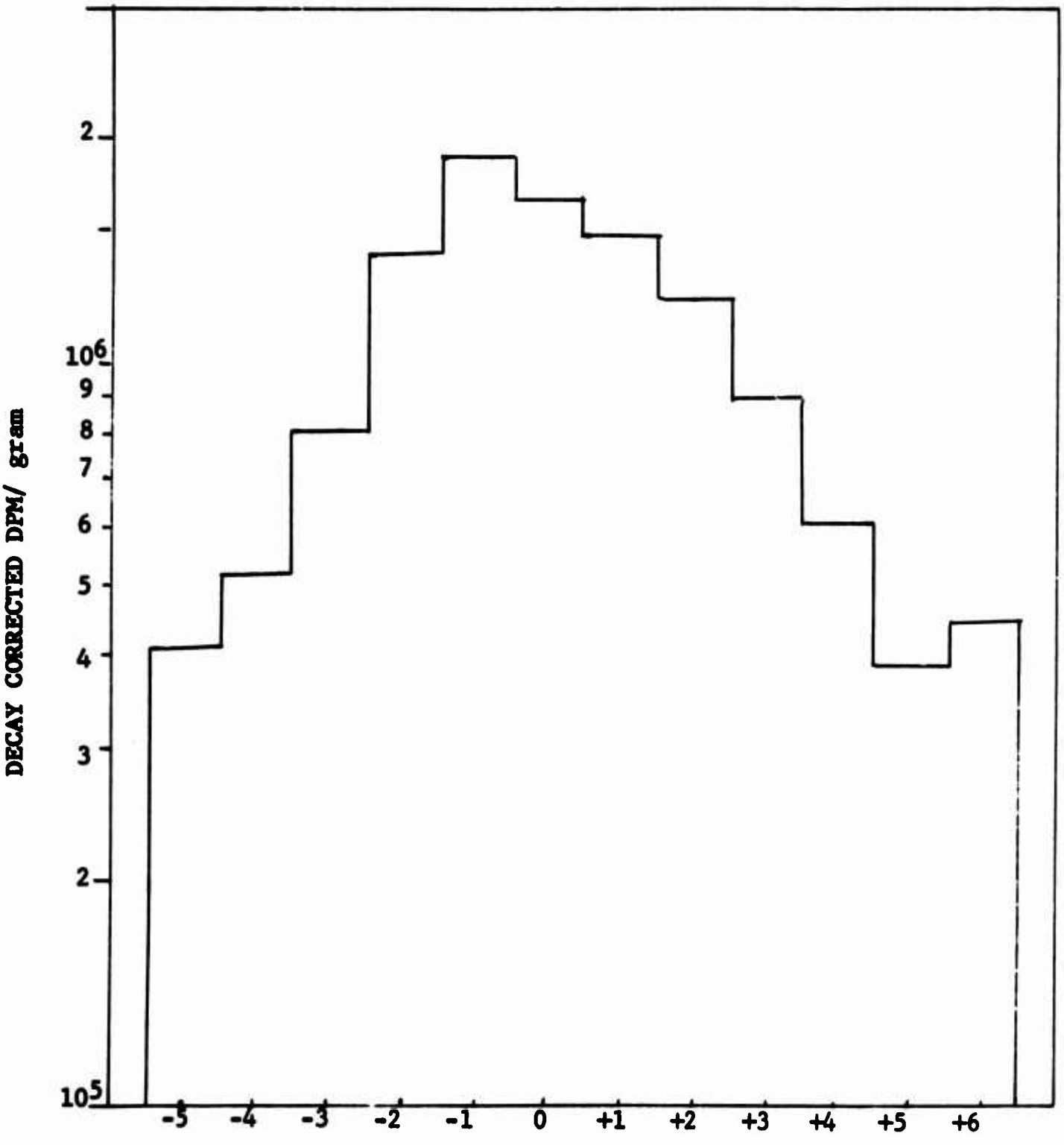

Figure 9. Ni^{57} Activity from $Ni^{58}(n,2n)Ni^{57}$ Across Radius of Target, 7/10/67

would be expected because the neutron flux density should be greatest at the center, becoming less as distance from the center increases. A feature that is unexplained is the activity of stip No. 11, which for both reactions was less than for strip No. 12. It may be that the lower activity resulted from the geometry involved. There may have been some water coolant, for example, affecting the average neutron energy at that part of the target. The ratio of saturation activities is of great interest, as it reflects the neutron energy. The ratio of cross sections as given by Barrall and McElroy (Ref. 6) for the reactions $Ni^{58}(n,p)Co^{58}$ and $Ni^{58}(n,2n)Ni^{57}$ is plotted as a function of neutron energy in Figure 10.

Thus if it is assumed that all the neutrons are D,T neutrons, one can use the ratio of saturation activities to measure energy of the neutrons. For example, strip No. 5, which had the highest activity, gave a ratio of 13.0, which corresponds to a neutron energy of 14.34 MeV. Strip No. 11, which had the lowest activity, gave a ratio of 16.0, which corresponds to a neutron energy of 14.15 MeV. The neutron energy is highest at the center. As distance from the center increases, the neutron energy decreases. This would be expected because the angle would be much greater toward the end positions. Finally, one would expect the energy of the neutrons striking the strip to be less than that striking the foils at a distance of 1 meter, because at a distance of 1 meter the angle is nearly 0°, whereas adjacent to the target, there is a wide range of angles. These considerations are generally confirmed by the data.

4. Measurement of Energy and Flux Density of D,T Neutrons at 1 Meter

To determine the energy of neutrons striking the foils on the large disc 1 meter from the target, a study was made of the reactions $Al^{27}(n,\alpha)Na^{24}$ and $Ni^{58}(n,2n)Ni^{57}$.

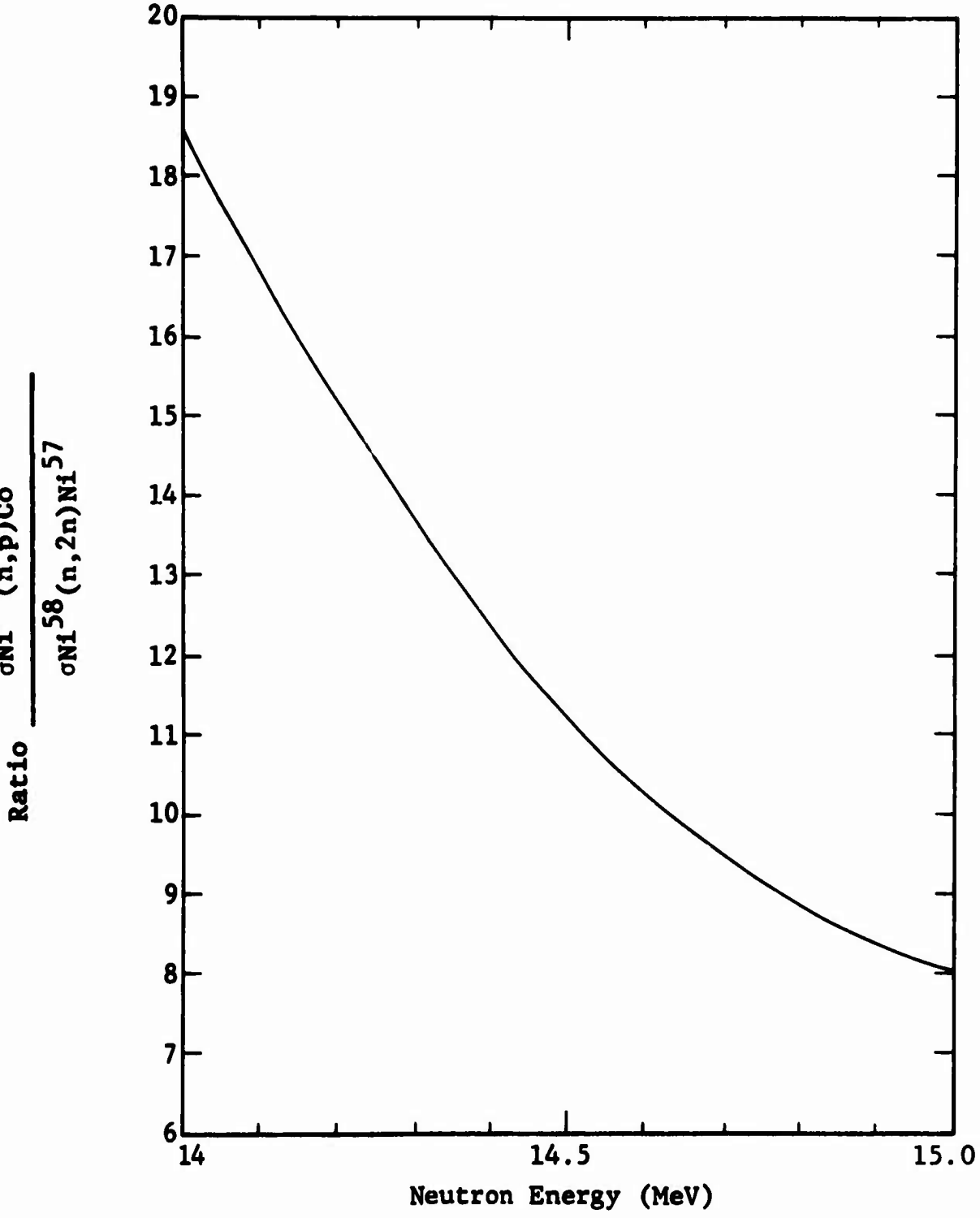

Figure 10. Energy Dependence of the Ratio of Cross Sections or Saturated Activities of $Ni^{58}(n,p)Co^{58}/Ni^{58}(n,2n)Ni^{57}$

TABLE X

Decay-Corrected Activities in Foils 1 meter from the Target, HENRE Run No. 40, 7/10/67.

Reaction	Average measured activity (DPM/gram)	Activity at saturation (DPS/nucleus x 10^{18})	Activity at saturation caused only by D,T neutrons (DPS/nucleus x 10^{18})
$F^{19}(n,2n)F^{18}$	783000	1.16	1.16
$Na^{23}(n,\gamma)Na^{24}$	3406	.415	(.364)*
$Na^{23}(n,2n)Na^{22}$	68.4	1.23	1.23
$Mg^{24}(n,p)Na^{24}$	294131	4.82	4.82
$Al^{27}(n,\alpha)Na^{24}$	209635	3.00	3.00
$S^{34}(n,\alpha)Si^{31}$	42900	3.42	2.86
$S^{32}(n,p)P^{32}$	14400	5.76	4.46
$Cl^{35}(n,\alpha)P^{32}$	4818	2.68	2.68
$Mn^{55}(n,\gamma)Mn^{56}$	62599	.356	(.186)
$Mn^{55}(n,2n)Mn^{54}$	1364	19.5	19.5
$Fe^{54}(n,p)Mn^{54}$	37.6	9.38	8.61
$Fe^{56}(n,p)Mn^{56}$	446494	2.81	2.81
$Co^{59}(n,\gamma)Co^{60}$	13.2	1.24	(0.55)
$Co^{59}(n,2n)Co^{58}$	5427	18.9	18.9
$Ni^{58}(n,np)+(n,d)Co^{57}$	941	18.2	18.2
$Ni^{58}(n,p)Co^{58}$	1838	9.388	8.48
$Ni^{58}(n,2n)Ni^{57}$	7634	.8293	.8293
$Cu^{65}(n,2n)Cu^{64}$	238500	22.3	22.3
$Cu^{63}(n,\alpha)Co^{60}$	8.37	1.23	1.23
$Zn^{64}(n,p)Cu^{64}$	62921	3.83	3.66
$Zr^{90}(n,2n)Zr^{89}$	40385	19.7	19.7
$In^{115}(n,2n)In^{114m}$	6641	33.0	33.0
$In^{115}(n,n')In^{115m}$	169290	3.44	1.66
$I^{127}(n,2n)I^{126}$	30914	41.6	41.6
$Au^{197}(n,2n)Au^{196G}$	50800	51.4	51.4
$Au^{197}(n,\gamma)Au^{198}$	82020	36.3	(16.6)
$Th^{232}(n,f)$Tracks	1957000**	12.6	11.1
$Th^{232}(n,f)[Mo^{99}]$	2510000	16.1	14.2
$U^{235}(n,f)[Mo^{99}]$	10970000**	71.34	(63.88)
$U^{238}(n,f)$Tracks	5555000**	36.6	30.8
$U^{238}(n,f)[Mo^{99}]$	5230000**	34.4	28.9

* = Values in parenthesis show effect of additional low energy neutrons.

** = Fissions/min-gram

By comparing the ratio of saturation activities for the two reactions with the cross section ratio at different energies, one may deduce an energy value for the D,T neutrons. Because neither of these reactions is induced by low-energy neutrons, any such "impurity" neutrons in the emitted spectrum will not introduce errors in the energy determination. On the other hand, the reaction $Ni^{58}(n,p)Co^{58}$, used in measuring the energy of neutrons hitting the nickel strip next to the target, has a threshold energy of approximately 1 MeV. Thus low-energy neutrons, if present, would cause an increase in the activity of Co^{58}.

Table X, which lists the activities measured in the foils irradiated at 1 meter, gives saturation activities of $.829 \times 10^{18}$ DPS/nucleus for $Ni^{58}(n,2n)Ni^{57}$ and 3.00×10^{18} DPS/nucleus for $Al^{27}(n,\alpha)Na^{24}$. The ratio of saturation activities is thus 3.62. By referring to Figure 11, one notes that this activity is thus corresponds to a neutron energy of 14.6 MeV. This result is several hundred KeV lower than one calculates based on a thin target, using the relativistic calculations of Blumberg and Schlesinger (Ref. 7).

5. Cross-Section Measurements

Table X lists the activities measured in foils on the large rotating disc. Note that all foils were irradiated simultaneously while at a distance of 1 meter from the target source. Therefore, the ratios of the saturated activities are proportional to the relative cross sections. By selecting one known cross-section value, all the measured cross sections may be obtained. The $Al^{27}(n,\alpha)Na^{24}$ cross section of 0.1207 barns at 14.6 MeV was used because this reaction is reliably measured and the cross section in this energy region is well known (Ref. 5). The values obtained are tabulated in Table XI.

Corrections were made for low-energy neutrons at an energy of 2.73 MeV for D,D neutrons; 2.58 MeV for the $Cu^{65}(n,2n)Cu^{64}$

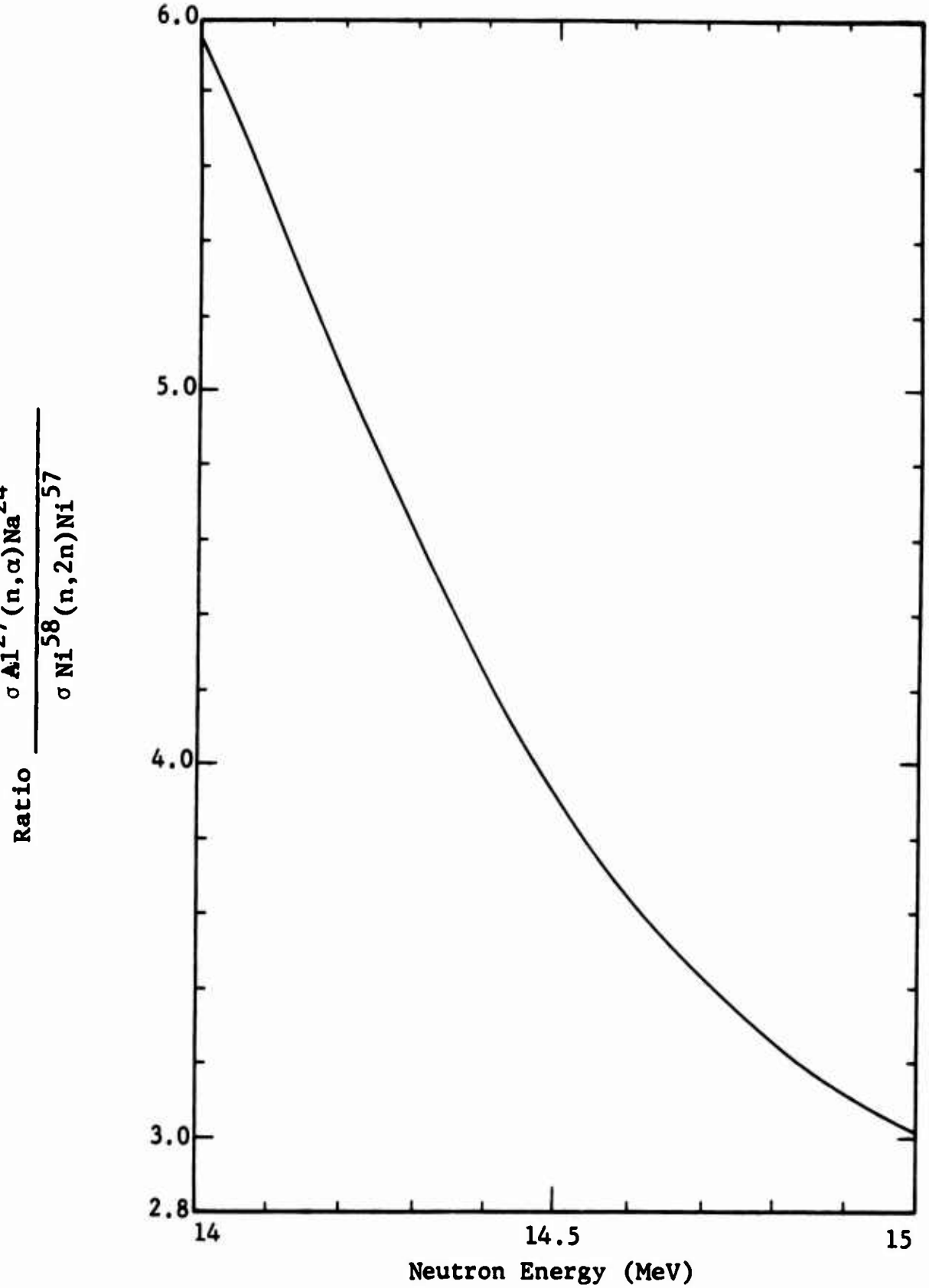

Figure 11. Energy Dependence of the Ratio of Cross Sections or Saturated Activities of $Al^{27}(n,\alpha)Na^{24}/Ni^{58}(n,2n)Ni^{57}$

TABLE XI

Measured Cross Sections at 14.6 MeV ± 0.2 MeV,
HENRE Run No. 40, 7/10/67.

Reaction	Cross Section (Barns)
$F^{19}(n,2n)F^{18}$	.047 ±.04
$Na^{23}(n,2n)Na^{22}$	.0495 ±.01
$Mg^{24}(n,p)Na^{24}$	.194 ±.014
$Al^{27}(n,\alpha)Na^{24}$	(.1207)*
$S^{34}(n,\alpha)Si^{31}$	.137 ±.01
$S^{32}(n,p)P^{32}$	.214 ±.016
$Cl^{35}(n,\alpha)P^{32}$	.108 ±.09
$Mn^{55}(n,2n)Mn^{54}$	.785 ±.08
$Fe^{54}(n,p)Mn^{54}$	.346 ±.03
$Fe^{56}(n,p)Mn^{56}$	.113 ±.08
$Co^{59}(n,2n)Co^{58}$	.760 ±.06
$Ni^{58}(n,np)+(n,d)Co^{57}$	.73 ±.06
$Ni^{58}(n,p)Co^{58}$	.341 ±.03
$Ni^{58}(n,2n)Ni^{57}$	.0334 ±.002
$Cu^{65}(n,2n)Cu^{64}$	.897 ±.10
$Cu^{63}(n,\alpha)Co^{60}$	.0495 ±.01
$Zn^{64}(n,p)Cu^{64}$	.147 ±.01
$Zr^{90}(n,2n)Zr^{89}$	.793 ±.06
$I^{127}(n,2n)I^{126}$	1.67 ±.09
$In^{115}(n,2n)In^{114m}$	1.33 ±0.12
$In^{115}(n,n')In^{115m}$	.067 ±.007
$Au^{197}(n,2n)Au^{196G}$	2.07 ±.2
$Th^{232}(n,f)$Tracks	.45 ±.04
$Th^{232}(n,f)[Mo^{99}]$	.56 ±.14
$U^{238}(n,f)$Tracks	1.24 ±.06
$U^{238}(n,f)$ $[Mo^{99}]$	1.16 ±.23

* Assumed Value

reaction; and at an energy of 2.20 MeV for the $Cu^{63}(n,2n)Cu^{62}$ reaction. Thus for each reaction listed in Table X the activity caused by low-energy neutrons was subtracted to obtain a saturation activity caused by D,T neutrons. These corrected activities were used in calculating the measured cross section.

6. Gold in Polysphere

A study was made of neutron attenuation in plastic by placing a series of gold foils at various distances throughout a polysphere. The gold foils used measured 0.5-inch in diameter, and were 0.004-inch thick. Following irradiation, measurements were made of the activity of Au^{198} in each foil. Table XII lists the activities, decay-corrected to time at end of irradiation, and also an estimate of the activity of Au^{196} interference. Figure 12 shows Au^{198} activity as a function of sphere thickness.

7. $B_4^{10}C$ Studies

Studies were also made on attenuation due to boron. A second rotating disc was positioned beneath the large rotating disc at a distance of 1.24 meters from the target source. On this rotating disc were placed $B_4^{10}C$ balls containing small thin foils of copper, gold, nickel and sulfur. The B^{10} used had a thickness of 1.4 grams/cm^2.

Following irradiation, activities were measured and data obtained for both shielded and unshielded activities.

Results for the reaction $S^{32}(n,p)P^{32}$ are shown in Figure 13. The P^{32} data were obtained relative to two unshielded pellets rotating on the same disc and at the same level as the center of the sphere. The $Ni^{58}(n,p)Co^{58}$ centered in the sphere and facing the source indicated a transmission of 0.95 while the gold and copper were not interpretable because of low-energy neutron interference.

TABLE XII

ACTIVITY OF Au^{198} AND Au^{196} IN GOLD FOILS IRRADIATED WITHIN A POLYSPHERE

Sphere Diameters (inches)	Activity Au^{198} (DPM/gram)	Estimated Activity Au^{196} (DPM/gram)
0	10971	300
2	78145	80
3	237673	trace
5	598717	trace
8	783553	trace
10	766355	none
12	676621	none

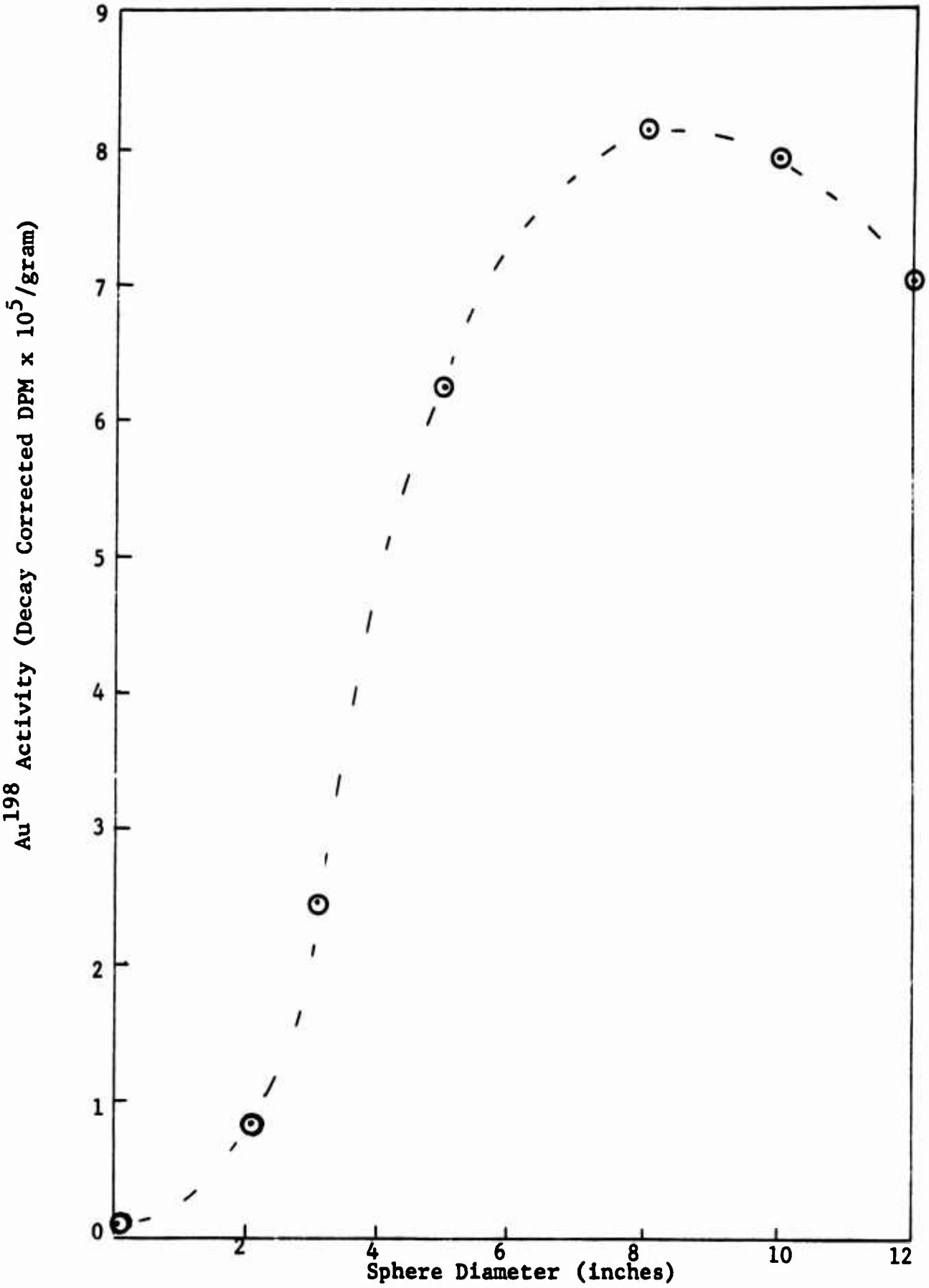

Figure 12. Gold Foils in Polysphere, HENRE Run No. 40.

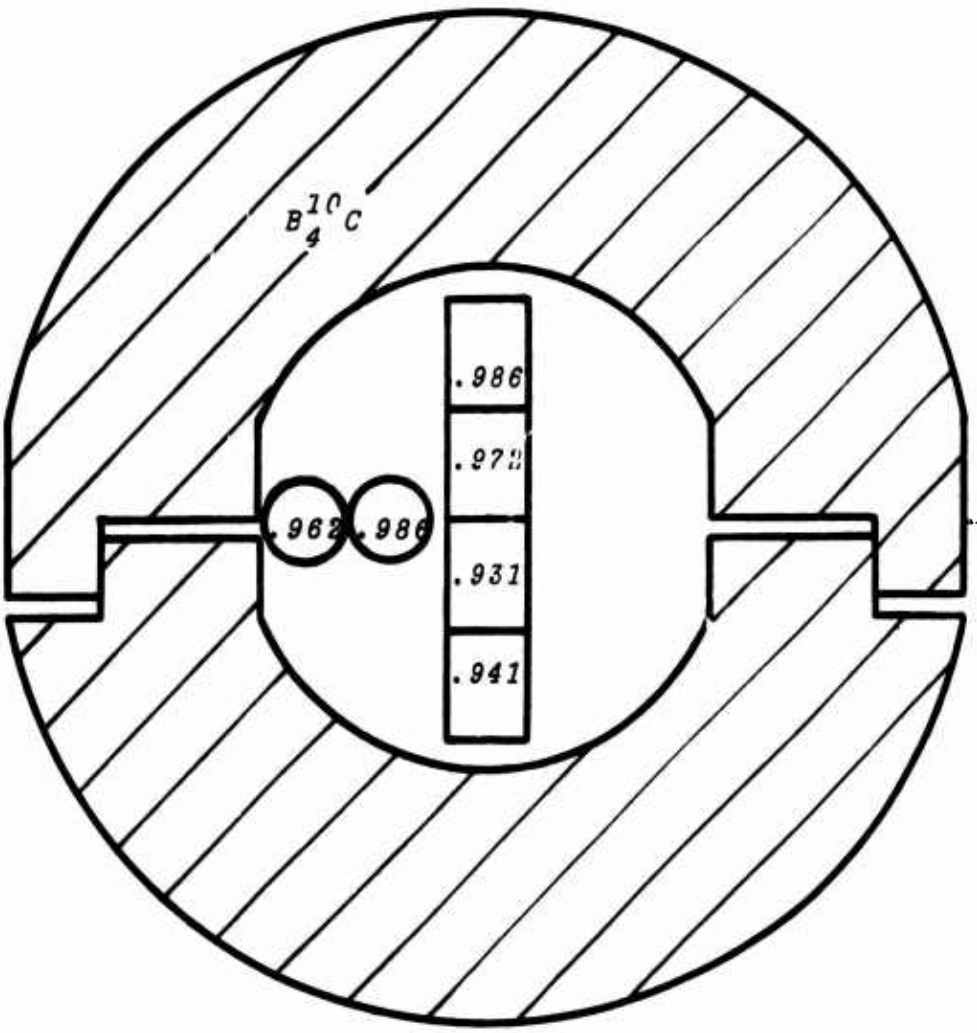

Figure 13. Neutron Attenuation in $B_4^{10}C$ Sphere As Measured by Using $S^{32}(n,p)P^{32}$

SECTION VI

IRRADIATIONS AT THE ICT, LAWRENCE RADIATION LABORATORY

1. Introduction

The purpose of the irradiations at the Lawrence Radiation Laboratory was to study the effects of low-energy D,D neutrons emitted along with the approximately 15 MeV D,T neutrons. This problem was deemed worthy of an investigation following the irradiations at the HENRE test site where it became evident that a considerable number of low-energy neutrons were emitted in addition to the D,T neutrons. These low-energy neutrons cause an increased activity for those reactions having an appreciable cross section for low-energy neutrons, but would not influence such reactions as $Al^{27}(n,\alpha)Na^{24}$ and $Ni^{58}(n,2n)Ni^{57}$, which have a high threshold energy.

2. Method

A newly fabricated target was prepared at Lawrence Radiation laboratory, and a series of consecutive irradiations were performed. On May 13, 1968, the first irradiation began at the instant the power was turned on. This irradiation lasted for approximately 10 minutes, and was followed by three more irradiations each of approximately 20 minutes, and finally by a 2-hour irradiation (runs 1 to 5). Then on June 26, 1968 when the target could be considered old, there were two more irradiations each of approximately 1-hour duration (runs 6 and 7).

Foils irradiated and the nuclear reactions studied are listed in Table XIII. All foils were placed on a single large rotating disc placed 14.5 $\pm$ 0.5 inches from the target. During irradiation the disc was rotated slowly with all foils on the same radius, the center of each foil being 6.5 inches from the

TABLE XIII

FOILS IRRADIATED AND REACTIONS STUDIED AT ICT

Foil Material	Reaction	Photon Energy Analyzed (MeV)	Photons per Disintegration
Al	$Al^{27}(n,\alpha)Na^{24}$	1.37	1.00
S	$S^{32}(n,p)P^{32}$	--	--
Fe	$Fe^{56}(n,p)Mn^{56}$	0.845	0.99
	$Fe^{54}(n,p)Mn^{54}$	0.835	1.00
Ni	$Ni^{58}(n,p)Co^{58}$	0.810	0.99
	$Ni^{58}(n,2n)Ni^{57}$	1.37	0.86
In	$In^{115}(n,n')In^{115m}$	0.335	0.50
I	$I^{127}(n,2n)I^{126}$	0.386	0.34
Au	$Au^{197}(n,\gamma)Au^{198}$	0.412	0.956

0° axis. Thus, the midpoint of each foil was at an angle of about 26°. In the case of a thin target, the neutrons produced by the D,T reaction would have an energy of 15.0 MeV.

Foils of a given material were of the same thickness and, except for the gold foil, all measured 3 in. x 3 in. configuration. The multichannel analyzer used for measuring the activity had previously been calibrated for foils of this size, using point source gamma ray standards from the National Bureau of Standards.

After irradiation, activities for all foils were measured and decay-corrected to time at end of irradiation. Saturated activity was then calculated for each reaction from each irradiation. These results are shown in Table XIV. The saturated activity for each foil was then compared with the average saturated activity measured from the reactions $Al^{27}(n,\alpha)Na^{24}$ and $Ni^{58}(n,2n)Ni^{57}$. Table XV lists these results.

A proton recoil telescope was used during these irradiations to measure the total number of coincidence counts. (See Table XVI). The proton recoil counter had a discriminator set to accept pulses only from neutrons with an energy greater than 9 or 10 MeV. Thus no low-energy neutrons were detected by these measurements. The number of neutrons per unit solid angle is given by the relation:

$$\text{No. neutrons/steradian} = \frac{\text{No. Coincidence Counts}}{6.61 \times 10^{-9}}$$

By using the inverse square law, the neutron flux density at the position of the foils (14.5 ± 0.5 inches from target) can be obtained from the relation:

$$\text{Neutron Flux density}(n/cm^2 sec) = \frac{\text{No. neutrons/steradian}}{\text{Time of irradia.(sec)} \times (14.5 \times 2.54)^2}$$

TABLE XIV

FOIL REACTIONS AND MEASURED ACTIVITIES AT ICT

Foil Reaction	Run No.	Ave. Measured Activity (DPM/gram)	Saturated Activity (DPS/nucleus x 10^{18})	Relative Sat. Activity*
$Al^{27}(n,\alpha)Na^{24}$	1	15260	1.482	1.000
	2	32524	1.585	1.070
	3	33616	1.624	1.096
	4	33783	1.646	1.111
	5	203496	1.717	1.159
	6	91861	1.361	.918
	7	104514	1.571	1.060
$In^{115}(n,n')In^{115m}$	1	6686	.8733	1.000
	2	14550	.9646	1.102
	3	14638	.9625	1.010
	4	14795	.9809	1.121
	5	83097	1.040	1.188
	6	38702	.8126	.928
	7	42073	.8957	1.023
$Ni^{58}(n,2n)Ni^{57}$	1	621	.4630	1.000
	2	1327	.4962	1.070
	3	1370	.5079	1.096
	4	1407	.5263	1.135
	5	8416	.5330	1.150
	6	3781	.4253	.917
	7	4215	.4914	1.060
$Ni^{58}(n,p)Co^{58}$	1	115	4.062	1.000
	2	247	4.379	1.078
	3	255	4.472	1.101
	4	259	4.586	1.129
	5	1600	4.727	1.164
	6	712	3.768	.928
	7	797	4.282	1.054
$S^{32}(n,p)P^{32}$	1	850	2.355	1.000
	2	1820	2.522	1.071
	3	1854	2.547	1.082
	4	1878	2.602	1.105
	5	11863	2.744	1.165
	6	5365	2.221	.943
	7	6010	2.525	1.072

* Normalized to Run No. 1 in each case.

3. Results

The reactions $Al^{27}(n,\alpha)Na^{24}$ and $Ni^{58}(n,2n)Ni^{57}$ can be looked upon as references because they are initiated only by high-energy neutrons. Those reactions induced by both high-energy and low-energy neutrons should have a relatively higher response as the target becomes older and emits more D,D neutrons. Table XV indicates this effect to be very small at the ICT. The reactions $S^{32}(n,p)P^{32}$, $Ni^{58}(n,p)Co^{58}$, $In^{115}(n,n')In^{115m}$ and $Au^{197}(n,\gamma)Au^{198}$ all have a relative response (saturated activity very slightly greater than 1.00 by the time of the fifth and sixth irradiations.

The energy of the D,T neutrons in runs 5 and 6 was measured in a manner similar to that used for HENRE, Run No. 40. Saturation activities for the reactions $Ni^{58}(n,2n)Ni^{57}$ and $Al^{27}(n,\alpha)Na^{24}$ were obtained from the measured activities. A saturation activity ratio was thus obtained and, by referring to a curve showing cross section ratio as a function of neutron energy, a neutron energy could be assigned. For Run 5 the saturation activities of 1.7173×10^{-18} and 0.5330×10^{-18} give a ratio of 3.222. This corresponds to a neutron energy of 14.79 MeV. The neutron flux density, based on the reaction $Al^{27}(n,\alpha)Na^{24}$ with a cross section of 0.1165 is calculated to be 14.55×10^{6} neutrons/cm^2-sec. For Run 6, the saturation values of 1.361×10^{-18} and 0.4253×10^{-18} gives a ratio of 3.200, corresponding to a neutron energy of 14.80 MeV. The flux density, based on the reaction $Al^{27}(n,\alpha)Na^{24}$ with a cross section of 0.1163 at 14.80 MeV, is calculated to be 11.55×10^{6} neutrons/cm^2-sec. For Run No. 5 the proton recoil telescope measurements gave a result of $14.79 \times 10^{6} \pm 7$ percent neutrons/cm^2-sec. The flux density measurement based on the $Al^{27}(n,\alpha)Na^{24}$ reaction (14.55×10^{6} n/cm^2-sec) is 1.6 percent lower.

TABLE XV

SATURATED ACTIVITY MEASURED FOR EACH FOIL RELATIVE TO $Al^{27}(n,\alpha)Na^{24}$

Run No.	$Al^{27}(n,\alpha)Na^{24}$	$Ni^{58}(n,2n)Ni^{57}$	$S^{32}(n,p)P^{32}$	$Ni^{58}(n,p)Co^{58}$	$In^{115}(n,n')In^{115m}$	Proton Recoil	$Au^{197}(n,\gamma)Au^{198}$ (moderated)
1	1.000	1.000	1.000	1.000	1.000	---	1.000
2	1.000	1.000	1.001	1.008	1.030	1.000	1.021
3	1.000	1.000	.987	1.005	1.003	1.005	0.973
4	1.000	1.022	.995	1.017	1.009	1.001	1.012
5	1.000	.993	1.006	1.004	1.025	1.011	1.014
6	1.000	.999	1.027	1.010	1.011	---	---
7	1.000	1.000	1.012	.995	.965	---	---

TABLE XVI

PROTON RECOIL TELESCOPE MEASUREMENTS

Run No.	Time of Irradiation (seconds)	Number of Coincidence Counts	Neutron Flux Density (n/cm^2 sec$X10^{-6}$)	Neutron Fluence ($n/cm^2 \times 10^{-6}$)
1	600	---	---	---
2	1200	145852	13.56	15912
3	1210.2	151415	13.95	16882
4	1200	155013	14.41	17292
5	7200	954608	14.79	106488
6	4020	---	----	---
7	3960	---	---	---

Table XVII lists the measured cross sections for Runs 5 and 6. The measured cross sections are in agreement within 2 percent whether based on the proton recoil data or relative to the $Al^{27}(n,\alpha)Na^{24}$ reaction as reported by Paulsen and Liskien (Ref. 9).

TABLE XVII

CROSS SECTIONS MEASURED AT THE ICT

Reaction	Saturation Activity (DPS/nucleus x 10^{18})	Measured Cross Section (Barns)
	14.79 MeV	
$Al^{27}(n,\alpha)Na^{24}$	1.717	.1161 ± .008
$Ni^{58}(n,2n)Ni^{57}$	.5330	.0361 ± .003
$Ni^{58}(n,np+n,d)Co^{57}$	11.30	.764 ± .06
$Ni^{58}(n,p)Co^{58}$	4.727	.320 ± .025
$S^{32}(n,p)P^{32}$	2.744	.186 ± .015
$In^{115}(n,n')In^{115m}$	1.040	.0703 ± .005
$In^{115}(n,2n)In^{114m}$	20.60	1.39 ± .11
	14.80 MeV	
$Al^{27}(n,\alpha)Na^{24}$	1.361	.1158*
$Ni^{58}(n,2n)Ni^{57}$	.4253	.0362 ± .003
$Ni^{58}(n,p)Co^{58}$	3.768	.321 ± .025
$Fe^{56}(n,p)Mn^{56}$	1.272	.1082 ± .009
$Fe^{54}(n,p)Mn^{54}$	3.507	.298 ± .024
$In^{115}(n,n')In^{115m}$	.8126	.0691 ± .005
$S^{32}(n,p)P^{32}$	2.221	.189 ± .015
$I^{127}(n,2n)I^{126}$	18.83	1.60 ± .13

* Assumed Value

REFERENCES

1. McElroy, W.N.; Barrall, R.C.; Ewing, D.; Neutron Flux Spectra Determination by Foil Activation; AFWL-TR-65-34, Vol. 1, Kirtland AFB, NM, August 1965. An Advanced Foil Activation Method of Determining Neutron Flux Spectra for Radiation Effects Studies.

2. McElroy, W.N.; Berg, S.; Crockett, T.; Hawkins, R.G.; A Computer-Automated Iterative Method for Neutron Flux Spectra Determination by Foil Activation, AFWL-TR-67-41, Vol. 1, Kirtland AFB, NM. September 1967.

3. Murphy, H.M. Jr.; PPA, A Computer Program for Photopeak Analysis, AFWL-TR-65-111, Kirtland AFB, NM. March 1966.

4. Heath, R.L.; Scintillation Spectrometry Gamma-Ray Spectrum Catalogue, IDO-16880-1, TID-4500, Vol. 1 of 2, USAEC, August 1964.

5. Pretre, S.; Tochilin, F.; Goldstein, N.; A Standardized Method for Making Neutron Fluence Measurements by Fission Fragment Tracks in Plastics. AD 643 540, Naval Radiological Defense Laboratory, San Francisco, Calif. Dec. 14, 1966.

6. Barrall, R.C.; McElrcy, W.N.; Neutron Flux Spectra Determination by Foil Activation: Experimental and Evaluated Cross Section Library of Selected Reactions. AFWL-TR-65-34, Vol. II, Kirtland AFB, NM. August 1965.

7. Blumberg, L.; Schlesinger, S.; Relativistic Tables of Energy and Angle Relationships for the $T(p,n)He^3$, $D(d,n)He^3$ and $T(d,n)He^4$ Reactions, (AECU-3118) Los Alamos Scientific Laboratory, Los Alamos, NM. May 1956

8. Armani, R.J.; Absolute Determination of Fission Rates in ^{235}U and ^{238}U by Radiochemical Techniques. Proceedings of a Symposium, Vienna, 10-14 October 1966, pp. 613-618.

9. Paulsen, A., and Liskien, H., Journal of Nuclear Energy Parts A/B. Vol. 19, 1965, pp. 907-911.

UNCLASSIFIED

Security Classification

DOCUMENT CONTROL DATA - R & D

(Security classification of title, body of abstract and indexing annotation must be entered when the overall report is classified)

1. ORIGINATING ACTIVITY (Corporate author)	2a. REPORT SECURITY CLASSIFICATION
Stanford University Stanford, California	UNCLASSIFIED
	2b. GROUP

3. REPORT TITLE

HIGH ENERGY NEUTRON CROSS SECTION VALIDATION AND NEUTRON FLUX SPECTRUM USING THE HENRE SOURCE

4. DESCRIPTIVE NOTES (Type of report and inclusive dates)

November 1965 to October 1968

5. AUTHOR(S) (First name, middle initial, last name)

Raymond, C. Barrall; John A. Holmes; Mae Silbergeld

6. REPORT DATE	7a. TOTAL NO. OF PAGES	7b. NO. OF REFS
March 1969	72	9

8a. CONTRACT OR GRANT NO.	9a. ORIGINATOR'S REPORT NUMBER(S)
AF 29(601)-6780	
b. PROJECT NO. 1831	AFWL-TR-68-134
c. Task: 08	9b. OTHER REPORT NO(S) (Any other numbers that may be assigned this report)
d.	

10. DISTRIBUTION STATEMENT

This document has been approved for public release and sale; its distribution is unlimited.

11. SUPPLEMENTARY NOTES	12. SPONSORING MILITARY ACTIVITY
	AFWL (WLBN) Kirtland AFB, NMex. 87117

13. ABSTRACT (Distribution Limitation Statement No. 1)

Neutron cross sections reported by various investigators often differ far in excess of the estimates of error reported. The high neutron emission of the High Energy Neutron Reaction Experiment (HENRE) source, 10^{13} n/sec, afforded an opportunity to compare measured values of many disintegration rates in a single experiment thus eliminating some of the uncertainty necessarily associated with such measurements when based on varying standards and normalizations. From these measurements, the 14.6 MeV neutron cross sections of 24 reactions are derived. The neutron spectrum near ground level at 37 feet slant range from the HENRE source was measured by using foil data and SAND II code. Additional measurements at the Insulated Core Transformer (ICT) accelerator at the Lawrence Radiation Laboratory, Livermore, served to confirm the HENRE results.

DD FORM 1 NOV 65 1473

UNCLASSIFIED

Security Classification

14. KEY WORDS	LINK A		LINK B		LINK C	
	ROLE	WT	ROLE	WT	ROLE	WT
Activation cross section Threshold foils Neutron spectra Operation HENRE SAND I Computer Code RADIAC						